

LLM-Empowered Agentic MAC Protocols: A Dynamic Stackelberg Game Approach

Renxuan Tan, Rongpeng Li, Fei Wang, Chenghui Peng, Shaoyun Wu, Zhifeng Zhao, and Honggang Zhang

Abstract—Medium Access Control (MAC) protocols, essential for wireless networks, are typically manually configured. While deep reinforcement learning (DRL)-based protocols enhance task-specified network performance, they suffer from poor generalizability and resilience, demanding costly retraining to adapt to dynamic environments. To overcome this limitation, we introduce a game-theoretic LLM-empowered multi-agent DRL (MARDL) framework, in which the uplink transmission between a base station and a varying number of user equipments is modeled as a dynamic multi-follower Stackelberg game (MFSG), capturing the network’s natural hierarchical structure. Within this game, LLM-driven agents, coordinated through proximal policy optimization (PPO), synthesize adaptive, semantic MAC protocols in response to network dynamics. Protocol action grammar (PAG) is employed to ensure the reliability and efficiency of this process. Under this system, we further analyze the existence and convergence behavior in terms of a Stackelberg equilibrium by studying the learning dynamics of LLM-empowered unified policies in response to changing followers. Simulations corroborate that our framework achieves a 77.6% greater throughput and a 65.2% fairness improvement over conventional baselines. Besides, our framework generalizes excellently to a fluctuating number of users without requiring retraining or architectural changes.

Index Terms—Protocol Emergence, Large Language Models, Stackelberg Game, Reinforcement Learning

I. INTRODUCTION

The evolution towards next-generation (xG) wireless systems envisions artificial intelligence (AI)-native architectures wherein intelligent, resilient communication protocols autonomously emerge to manage unprecedented network dynamics [1]. Central to this vision is the medium access control (MAC) protocol, which orchestrates channel access among numerous nodes. As network topologies become increasingly varying and heterogeneous, the prevailing paradigm of designing static, human-engineered MAC protocols is rendered obsolete, necessitating protocol emergence solutions that can learn and adapt in real-time [2]. This need is particularly acute in challenging scenarios such as uplink data transmission scheduling (UDTS) within cellular networks [3], [4].

Deep reinforcement learning (DRL) and its multi-agent counterpart (MARDL) have become a promising approach in

this domain, modeling network nodes – such as base stations (BSs) and user equipments (UEs) – as autonomous agents that learn coordinated control messages and policies through trial-and-error interaction [5]–[8]. Despite substantial potential for enhancing network key performance indicators (KPIs), up-to-date formulations often neglect the intrinsic game-theoretic relationships among network entities, typically resorting to fully centralized or fully decentralized control paradigms [9], [10]. For instance, the uplink scheduling between a BS and its UEs is an inherently hierarchical game. Rigid, centralized control by BS stifles the ability of UEs to adapt rapidly to their time-varying local states. The Stackelberg game (SG), a canonical model for hierarchical interactions, more precisely captures these asymmetric dynamics [11] and can guide policy convergence in MARDL frameworks [12], rendering it a more natural and faithful solution. However, generalization in dynamic network environments remains a critical bottleneck [13], as fluctuating numbers of agents render traditional game-theoretic solutions and fixed-architecture MARDL methods infeasible.

Recently, characterized by impressive comprehension and generative reasoning capabilities, large language models (LLMs) have emerged as a compelling solution to intractable protocol design challenges [14]. Their inherent ability for processing variable-length sequences suggests a natural aptitude for operating in dynamic game environments, overcoming the architectural rigidity of non-LLM methods [10]. Nevertheless, instantiating SG agents with LLMs introduces unique challenges. A fundamental discrepancy arises between the pre-training objective of an LLM – generating plausible text – and the strategic reasoning needed for a leader or follower in an SG, which is to maximize network utility. Addressing this significant gap requires functional alignment of model behavior with strategic goals. Existing LLM-based systems, however, typically depend on meticulously curated, domain-specific datasets or expert prompt engineering for domain adaptation [15]. This dependency constrains their capacity for exploratory learning, the very mechanism required for the emergence of novel, high-performance protocols. Furthermore, bridging the semantic gap between the LLMs’ open-domain vocabulary and the game action space of MAC protocols is essential yet nontrivial. Reconciling generalization, exploration, and structured action generation is therefore critical [16] for achieving stable and efficient policy convergence in such dynamic game settings.

To overcome the limitations above, we propose an LLM-empowered MARDL framework that conceptualizes the MAC protocol emergence for UDTS as a dynamic multi-follower

R. Tan and R. Li are with the College of Information Science and Electronic Engineering, Zhejiang University, Hangzhou 310027, China. (email: {trrx, lirongpeng}@zju.edu.cn).

Fei Wang, Chenghui Peng, and Shaoyun Wu are with Huawei Technologies Company Ltd., Shanghai 210026, China. (email: {wangfei76, pengchenghui, wushaoyun}@huawei.com).

Z. Zhao is with Zhejiang Lab as well as Zhejiang University, Hangzhou 310027, China. (email: zhaozf@zhejianglab.org).

H. Zhang is with Macau University of Science and Technology, Macau, China (email: hgzhang@must.edu.mo).

Corresponding Author: Rongpeng Li

Stackelberg game (MFSG). This game is instantiated through LLM-empowered agents, where the BS serves as the leader agent and broadcasts a macroscopic scheduling intent as downlink control messages (DCMs). The UEs, acting as followers, interpret this intent in the context of their local observations and articulate their best responses as uplink control messages (UCMs). Crucially, we reformulate the MARL paradigm by endowing both the BS and UEs with language-oriented policy models that naturally handle variable-length input and output sequences while retaining the exploratory capabilities of DRL. We employ proximal policy optimization (PPO) to facilitate a continuous, feedback-driven alignment of the agents' policies with evolving network dynamics. This synergistic design overcomes the architectural rigidity of conventional MARL and mitigates the data dependency of LLMs. We also incorporate a protocol action grammar (PAG) to guarantee reliability and efficiency by enforcing domain-specific constraints on agent decisions. To this end, we theoretically analyze the convergence of an equilibrium within this learning framework. We summarize the key differences between our algorithm and highly related literature in Table I.

Our key contributions are threefold, as follows.

- We establish a dynamic MFSG formulation for MAC protocol emergence in the UDS scenario, explicitly capturing the inherently hierarchical interactions between BS and a dynamically varying number of UEs. As a pioneering effort, this game-theoretic model fundamentally differs from existing paradigms [3], [4] by formulating asymmetric leader-follower relationships.
- We propose a novel LLM-empowered MARL framework that fundamentally reconciles the powerful generalization capabilities of LLMs with the exploratory learning essential for protocol discovery, driven by PPO. The concerted effort makes our design uniquely capable of adapting to a dynamic network without retraining. It also incorporates a PAG mechanism to further enhance efficiency and reliability.
- We provide a theoretical analysis of our framework, including the guaranteed existence of a Stackelberg equilibrium (SE) in the dynamic game, and the local convergence of our learning algorithm to this equilibrium. Extensive simulations have validated the superiority and robustness of our proposed algorithm.

This paper is structured as follows. Section II details the related works. Section III presents the system model and formulates the problem. Section IV details the LLM-based decision maker and its PPO training. Section V evaluates performance via simulations, and the main conclusion is drawn in Section VI.

II. RELATED WORKS

A. DRL for Communication Protocol

Leveraging its data-driven exploration and trial-and-error mechanisms, DRL is suited to optimize and even discover protocols for task-specific applications. One research line focuses on optimizing the functional blocks and operational parameters of existing protocols [20], [25]–[28]. For example, Ref. [25],

[26] introduce DRL to automatically revise the features of protocol blocks in response to various network conditions, demonstrating superior throughput and latency compared to traditional methods. Ref. [27] proposes specialized wireless networks (SpecNets), wherein agents dynamically adjust settings such as contention windows and frame aggregation to meet diverse performance demands. Another research thrust focuses on augmenting the adaptability of communication protocols. Ref. [28] proposes the MARL-based QLBT protocol, demonstrating its adaptability across various dynamic network conditions and coexistence scenarios. Ref. [20] employs multi-task learning and a scalable transformer-based critic to train a single, generalizable model that can adapt to dynamic network sizes and traffic conditions. In contrast, several works have considered protocol emergence through training from scratch. Ref. [3] establishes a DRL framework to learn channel access policies and signaling simultaneously. Subsequent works extend this with more advanced MARL algorithms and optimization tricks [5], [6], [8], [9], achieving notable progress in the convergence, adaptability, and scalability of emergent protocols. Ref. [22] even explores interpretability by encoding symbolic structure via a probabilistic logic programming language (ProbLog). Nevertheless, a persistent challenge for existing DRL-based solutions is their limited generalization [23], rendering them brittle in highly dynamic network environments and often necessitating costly retraining or architectural redesigns.

B. LLMs for Communication Protocol

The advent of LLMs is set to revolutionize wireless protocol design. Benefiting from their remarkable capabilities in understanding, reasoning, and generalization, alongside their extensive general knowledge bases, LLMs have achieved considerable success in various downstream tasks within wireless networking [29]. On the one hand, LLMs can serve as base models that are fine-tuned on communications-specific datasets to support resource management [30], standard-protocol interpretation [31], and protocol design [18], [19]. On the other hand, LLMs also facilitate direct zero-shot or few-shot domain adaptation. Ref. [21] leverages knowledge acquired via in-context learning and uses knowledge distillation to guide and accelerate protocol emergence in multi-agent navigation systems. Recently, Ref. [24] employs prompt engineering to auto-tune LLM system prompts for generating semantic signaling tokens for BSs and UEs, enabling zero-shot adaptation to environmental dynamics. Ref. [23] further showcases the coordination of agentic LLM workflows for autonomous and interpretable protocol design. While effective in achieving high performance, LLMs without post-training remain path-dependent on domain-specific datasets and highly engineered prompts, which constrain their ability to discover fundamentally new protocols through exploration. Our previous work [10] makes an initial attempt to reconcile exploration with generalization by fine-tuning an LLM-based policy using PPO. Yet, it fell short of capturing the intrinsic game-theoretic interactions among agents.

TABLE I
THE SUMMARY OF DIFFERENCES WITH RELATED LITERATURE ON PROTOCOL EMERGENCE.

	Exploratory Protocol Discovery	Dynamic Adaptability	Intrinsic Hierarchy Modeling	Semantic Protocols	Brief Description
[4]–[6], [9]	●	●	○	○	Vanilla DRL for protocol emergence
[17]	○	●	●	○	Static rules or datasets reliance result in insufficient exploration
[18], [19]	○	●	○	●	Ignoring signaling interpretability
[8], [20]	●	●	●	○	Ignoring intrinsic game theoretic formulation among network agents
[21]–[23]	●	●	○	●	Ignoring intrinsic game theoretic formulation among network agents
[24]	●	●	○	●	Ignoring intrinsic game theoretic formulation among network agents
Ours	●	●	●	●	Synergizes a dynamic Stackelberg game model with an LLM-RL policy to learn semantic emergent protocols that are adaptive to network dynamics

Notations: ○ indicates not included; ● indicates fully included; ● means partially included.

C. Stackelberg Game in Wireless Communication

Armed with an intrinsic leader-follower structure, SG has been widely used to capture hierarchical strategic interactions in wireless network domains like resource allocation and power control [32]–[35]. In [32], the SG framework effectively models the pricing strategies between service providers (leaders) and end-users (followers) in complex multi-tenant network slicing environments, demonstrating faster convergence and greater economic efficiency. Ref. [33] employs an SG to model energy trading between a power station and a transmitter in an intelligent reflection surface-aided wireless-powered multicast system, optimizing phase shifts to jointly maximize the utilities of both service providers. Ref. [34] extends this hierarchical modeling to a two-layer game, articulating the resource cascade from cloud service providers down to edge providers and end-users. The SG framework is also leveraged to strike an optimal balance between transmission performance and cost for source nodes and collaborative relays [35]. Accordingly, the leader-follower paradigm delineates the fundamental dynamics governing network interactions and even accelerates convergence [12], guiding agents toward a more efficient equilibrium. However, to our best knowledge, MFSG has not been leveraged to develop MAC protocols.

III. SYSTEM MODEL AND PROBLEM FORMULATION

A. System Model

1) *Basics of UDTS*: As illustrated in Fig. 1, we investigate a UDTS within a single-cell orthogonal frequency division multiple access (OFDMA) system where a BS serves multiple UEs. The set of I active UEs is denoted by $\mathcal{F}_t = \{u_1, \dots, u_I\}$ at time t , where I may vary due to the arrivals and departures of UEs, reflecting the dynamic nature of the network topology. Consistent with 3GPP TS 38.321 [36], the BS assigns each UE dedicated physical uplink/downlink control channels (PUCCH/PDCCH) for signaling and a shared contention-based channel (PUSCH) for MAC data protocol data unit (dPDU) transmission. The available bandwidth is divided into M orthogonal resource block groups (RBGs) in the frequency domain, and time is discretized into slots of fixed duration, termed as transmission time intervals (TTIs). An operational cycle, or episode, spans T TTIs. This scenario necessitates efficient MAC protocols that jointly optimize signaling and

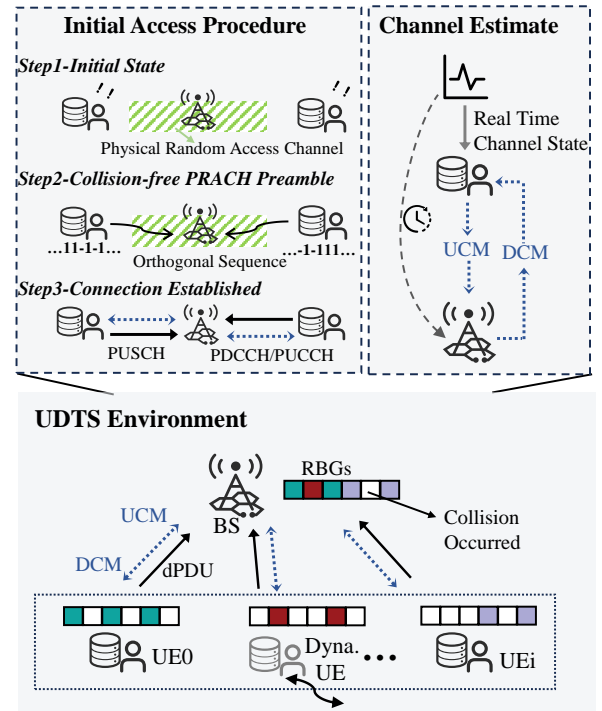


Fig. 1. Scenario of interest: A BS serves dynamic UEs within an OFDMA system, UEs select RBGs for dPDU transmission, coordinating with the BS via UCMs and DCMs.

access strategies to mitigate RBG collisions while balancing KPIs like throughput, resource efficiency, and fairness. At time slot t , UE u_i constructs and transmits a UCM $u_{i,t}$, encapsulating its local state (e.g., buffer status report and interaction history) and transmission intent. In response, the BS integrates these UCMs with its global observations to issue a DCM $d_{i,t}$ to each UE, conveying its macroscopic scheduling intent. These signaling exchanges, typically conveyed over the dedicated PUCCH and PDCCH, are crucial for coordinating access and establishing the operational context for data delivery.

2) *Delivery Model*: We model the arrival of new data at each UE as a Bernoulli process [3], [5], where a dPDU of a fixed size ξ^{gen} (in bits) is generated with probability p_a in each TTI. Meanwhile, each UE is equipped with a first-in-first-out (FIFO) buffer of capacity B_{cap} to temporarily store

TABLE II
NOTATIONS MAINLY USED IN THIS PAPER.

Notation	Description
I_t, \mathcal{J}_t	Number of active UEs and the set of UEs at time slot t
M	Number of RBGs
T	Number of TTIs per episode
ξ^{gen}	Generated dPDU size
$\xi_{i,t,u}^{\text{rec}}, \xi_{i,t,u}^{\text{tx}}$	dPDUs successfully received and total transmission attempts by UE u_i at time slot t
$u_i, d_{i,t}$	UCM and DCM of UE u_i at time slot t
$b_{i,t}$	Buffer occupancy of UE u_i at time slot t
$\nu_{i,t}$	Spectral efficiency of UE u_i at time slot t
$c_{i,t,u}, \hat{c}_{i,t,u}$	Locally channel quality of UE u_i at time slot t and corresponding BS's channel state estimate
$x_{i,t,u}$	Cumulative RBGs utilized by UE u_i up to time t
$o_{t,b}, \tilde{o}_{t,b}$	Observations of the BS at time slot t
$o_{i,t,u}, \tilde{o}_{i,t,u}$	Observations of the UE u_i at time slot t
$a_{t,b}, \tilde{a}_{t,b}$	BS's action at time slot t , i.e., DCMs to UEs
$a_{i,t,u}, \tilde{a}_{i,t,u}$	UE u_i 's action at time slot t , comprising a transmission bitmap $a_{i,t,u}^{\text{bit}}$ and a UCM
$F_{t,b}$	Utility function of the leader (BS) at time slot t
$F_{i,t,u}$	Utility function of the follower UE u_i at time slot t
$\pi_b, \pi_{i,u}$	Policies for the BS (leader) and UE u_i (follower)
$\mathbb{D}(\cdot)$	The probability distribution of the number of active UEs
θ_b, θ_u	Policy parameters for the BS and the shared UE network
$J_b(\cdot), J_{i,u}(\cdot)$	Expected long-term utilities for the BS and UE u_i
$\phi, L(\cdot)$	Parameters of critic network and TD error for its update
$V(\cdot), A(\cdot)$	State-value function and advantage function
γ, λ	Discount factor for long-term rewards and GAE
α, β	Learning rate for actor and critic update
e	Training epoch
ψ_b, ψ_u	Meta-prompts for the BS and UE LLM agents
$\tau_b, \tau_{i,u}$	Trajectory rollout of BS and UEs
$\mathcal{B}_b, \mathcal{B}_u$	Trajectory replay buffers for the leader and followers
$\mathcal{W}, \mathcal{W}^-$	LLM vocabulary and PAG-constrained vocabulary
Θ, Ω	Joint policy parameters and update gradient field

dPDUs, with the buffer occupancy denoted by $b_{i,t} \in [0, B_{\text{cap}}]$. The UE transmission action, denoted by $a_{i,t,u}^{\text{bit}}$, is an M -bit binary bitmap, where each bit indicates whether the m -th RBG is selected for data transmission. Following 3GPP TS 38.214 [37], the maximum transport block size (TBS) of u_i in time slot t is given by

$$N_{i,t,u} = \text{tr}(\mathbf{1}^T a_{i,t,u}^{\text{bit}}) \cdot N_{\text{rb}}^{\text{rbg}} \cdot N_{\text{sc}}^{\text{rb}} \cdot N_{\text{symbl}}^{\text{sh}} \cdot \nu_{i,t} \quad (1)$$

where $N_{\text{rb}}^{\text{rbg}}$ is the number of RBs per RBG, $N_{\text{sc}}^{\text{rb}}$ is the number of subcarriers per RB, $N_{\text{symbl}}^{\text{sh}}$ is the number of symbols per slot, and $\nu_{i,t}$ denotes spectral efficiency. Crucially, $\nu_{i,t}$ is a time-varying quantity that depends on the instantaneous signal-to-noise ratio (SNR) of the link and the corresponding modulation and coding scheme (MCS) selected by the UE. The system employs an automatic repeat request (ARQ) process for buffer management, ensuring UEs remove bits from their buffers after the BS confirms a successful data reception.

3) *Channel Model*: Without loss of generality, we model the PUSCH as a packet erasure channel with a nonzero transport block error rate (TBLER). If an RB is collision-free and the transmission is error-free, the BS successfully receives the transmitted data. Moreover, the channel quality for UE u_i at time t is denoted by $c_{i,t,u}$, which evolves between several discrete states. Its transitions reflect short-term channel fluctuations (e.g., fast fading) and thus affect the instantaneous spectral efficiency $\nu_{i,t}$. In parallel, the BS acquires corresponding channel state information (CSI), $\hat{c}_{i,t,u}$,

which may differ from the UE's locally true state. This discrepancy arises from a combination of factors, including estimation errors from imperfect channel reciprocity in a time division duplexing (TDD) system and inherent delays.

4) *Decision Model*: A sequential decision-making process governs both UE-BS signaling and the UE's transmission behavior. For each UE u_i , define its observation at time t as $o_{i,t,u} = (c_{i,t,u}, b_{i,t}, a_{i,t,u}, d_{i,t})$ whereas the taken action $a_{i,t,u} = (a_{i,t,u}^{\text{bit}}, u_{i,t})$. Meanwhile, the BS's observation is given by $o_{t,b} = (\{\hat{c}_{i,t,u}\}_{i \in \mathcal{J}_t}, \{u_{i,t}\}_{i \in \mathcal{J}_t}, \{d_{i,t}\}_{i \in \mathcal{J}_t})$ and its action is defined as $a_{t,b} = (d_{1,t}, \dots, d_{I,t})$. Notably, the macroscopic guidance, provided by the BS, could be the outcome of information disparities (e.g., the fast fading). Therefore, fine-grained adjustments from UEs based on their more accurate, real-time local observations can compensate for the imbalance with local execution efficiency. Crucially, both BS and UE observations are primarily composed of the preceding interactive UCMs/DCMs, which evolve into meaningful signaling messages during the training process, thereby dynamically refining UE behaviors to optimize system performance. Each agent's behavior is dictated by a policy that maps its observations to a probability distribution over the action space. Let π_b be the leader's policy and $\pi_{i,u}$ the follower's policy, such that $a_{t,b} \sim \pi_b(o_{t,b})$ and $a_{i,t,u} \sim \pi_{i,u}(o_{i,t,u})$.

B. Stackelberg Game Formulation

We formally model the sequential and interactive decision-making process as a dynamic MFSG to capture the inherent hierarchical relationship between the BS and UEs. In this game, the BS serves as the leader, making strategic decisions to optimize network-wide performance, while the UEs are followers that respond to the BS's actions to maximize their individual utilities. Our objective is to develop a framework that facilitates the emergence of leader-follower policies, driving the system toward a desirable SE.

Specifically, the utility for a follower $u_i \in \mathcal{J}_t$ at time slot t is defined as a weighted sum of transmission efficiency and its consistency with the leader's DCM:

$$F_{i,t,u} = \varrho_1 \cdot \frac{\xi_{i,t,u}^{\text{rec}}}{\xi_{i,t,u}^{\text{tx}}} + \varrho_2 \cdot C_{i,t,u}, \quad (2)$$

where ϱ_1, ϱ_2 are constants, $\frac{\xi_{i,t,u}^{\text{rec}}}{\xi_{i,t,u}^{\text{tx}}}$ denotes the successfully received dPDUs from u_i at time slot t , and $\xi_{i,t,u}^{\text{tx}}$ represents the total number of transmission attempts made by u_i . $C_{i,t,u}$ quantifies the normalized Hamming similarity [38] between the UE's transmission bitmap $a_{i,t,u}^{\text{bit}}$ and the BS's intended allocation bitmap $d_{i,t}^{\text{bit}}$ (i.e., the bit-level representation of $d_{i,t}$ and can be directly derived from $a_{t,b}$). In other words,

$$C_{i,t,u} = \frac{1}{M} \sum_{m=1}^M (1 - (a_{i,t,u,m}^{\text{bit}} \oplus d_{i,t,m}^{\text{bit}})). \quad (3)$$

Given the leader's policy π_b , each follower seeks to find its best-response policy $\pi_{i,u}^*$ that maximizes its expected discounted long-term utility $J_{i,u}$ over the distribution of UE numbers $\mathbb{D}(I)$,

$$J_{i,u} = \mathbb{E}_{I_t \sim \mathbb{D}(I)} \mathbb{E}_{\pi_{i,u}, \pi_b, \pi_{-i,u}} \left[\sum_{t=0}^{T-1} \gamma^t F_{i,t,u} \right], \quad (4)$$

where $\gamma \in [0, 1]$ is the discount factor. Conversely, the leader's utility $F_{t,b}$ aligns with the system-level objectives, defined as a weighted sum of the average user throughput and inter-user fairness:

$$F_{t,b} = \frac{1}{|\mathcal{J}_t|} \sum_{i \in \mathcal{J}_t} \xi_{i,t,u}^{\text{rec}} + \varepsilon \frac{(\sum_{i \in \mathcal{J}_t} x_{i,t,u})^2}{|\mathcal{J}_t| \cdot \sum_{i \in \mathcal{J}_t} (x_{i,t,u})^2}, \quad (5)$$

where the weighting factor ε controls the trade-off with fairness, which is quantified using Jain's Fairness Index (JFI) [39], $x_{i,t,u}$ represents the cumulative number of RBGs utilized by UE u_i up to time t . At this equilibrium, the leader's policy is a universal solution to Eq. (6), anticipating that all followers will adhere to their best-response policies.

$$\max_{\pi_b} J_b = \max_{\pi_b} \mathbb{E}_{I_t \sim \mathbb{D}(I)} \mathbb{E}_{\pi_b, \pi_u^*} \left[\sum_{t=0}^{T-1} \gamma^t F_{t,b} \right], \quad (6)$$

where $\pi_u^* = (\{\pi_{i,t,u}^*\}_{i \in \mathcal{J}_t})$.

Consequently, the problem is to find a set of policies $(\pi_{t,b}^*, \{\pi_{i,t,u}^*\}_{i \in \mathcal{J}_t})$ that constitutes an expected Stackelberg equilibrium (ESE) over $\mathbb{D}(I)$, where no player has an incentive to unilaterally deviate from their policy. Solving such an equilibrium is nontrivial due to the implicit coupling of utilities and the high-dimensional state-action space, which renders traditional optimization intractable. While MARL is a promising alternative, its fixed architectures fail to generalize to a dynamic environment. To address this, we propose an LLM-driven MARL framework that jointly leverages MARL's exploratory power and LLMs' generalization capability to learn robust equilibria, as detailed in the following section.

IV. PPO-BASED LLM DECISION MAKER FOR PROTOCOL EMERGENCE

In this section, we recast the search for the SE as an LLM-empowered multi-agent learning process, where all agents operate in a semantic-generalized UTDS environment. Both the BS and UEs leverage parameterized LLM as their decision-making policies. Within each TTI, based on its observation, the BS initiates its action $a_{t,b}$, and the UEs react accordingly. Ultimately, both agents receive their respective rewards from the environment. PPO with expert seeding is employed to ground the LLMs' performance, ensuring the policies are functionally aligned with the dynamic environment.

A. Framework of RL-based Protocol Emergence

We begin by outlining the conventional MARL approach for protocol emergence, establishing a baseline, and highlighting its limitations. Following the work [6], the UTDS is formulated as a decentralized partially observable Markov decision process (Dec-POMDP), where agents are trained concurrently to learn both transmission and signaling actions using PPO. The UCM and DCM are treated as special discrete actions of the UEs and the BS, respectively. While these signaling actions do not directly alter the environment, they influence the decisions of other agents by being part of their observable states. Taking the BS as an example, we illustrate its training process. As generally defined by the PPO framework, the BS owns an actor network to represent its policy π_b and a critic

network $V(o_{t,b})$ for its value function, parameterized by θ_b and ϕ_b respectively. The collective goal is to find a policy that maximizes the objective function defined in (6). During the interaction with the environment, the BS agent collects a series of experience trajectories τ composed of transition tuples and

$$\tau_b = \{(o_{t,b}, a_{t,b}, F_{t,b}, \pi_b(a_{t,b}|o_{t,b}), V(o_{t,b}), A_{t,b})\}_{t=0}^{|T-1|} \quad (7)$$

captures current observation, action, reward, policy probability, value estimate, and the advantage estimate. The advantage A_t is computed via generalized advantage estimation (GAE)

$$A_{t,b} = \sum_{l=0}^T (\gamma\lambda)^l (F_{t+l,b} + \gamma V(o_{t+l+1,b}) - V(o_{t+l,b})), \quad (8)$$

indicating whether an action taken is better or worse than the policy's average, and λ denotes the GAE factor. Updating the critic network ϕ_b involves minimizing the squared temporal-difference (TD) residuals

$$L(\phi_b) = \mathbb{E}_{\tau_b \sim \mathcal{B}_b} \left[\sum_{t=1}^T (V(o_{t,b}) - \hat{R}_{t,b})^2 \right], \quad (9)$$

where \mathcal{B}_b denotes experience buffers, $\hat{R}_t = \sum_{t'=t}^T \gamma^{t'-t} F_{t',b}$ is the discounted reward-to-go. The actor network θ_b^1 is updated via the sampled policy gradient from the clipped surrogate objective function

$$J(\theta_b) = \mathbb{E}_{\tau_b \sim \mathcal{B}_b} \left[\sum_{t=1}^T \left[\min(\eta_{t,b} A_{t,b}, \text{clip}(\eta_{t,b}, 1-\epsilon, 1+\epsilon) A_{t,b}) - D_{\text{KL}}(\pi_b^{\text{old}}(\cdot|o_{t,b}) || \pi_b(\cdot|o_{t,b})) + H((\pi_b(\cdot|o_{t,b})) \right] \right], \quad (10)$$

where $\eta_{t,b} = \frac{\pi_b(a_{t,b}|o_{t,b})}{\pi_b^{\text{old}}(a_{t,b}|o_{t,b})}$ denotes the important ratio, the operator $D_{\text{KL}}(\cdot || \cdot)$ computes the KL-divergence, the policy entropy H encourages exploration, meanwhile both the clipping function $\text{clip}(\cdot)$ and the hyperparameter ϵ prevent excessively large policy updates.

B. Semantic-Generalized MFSG

It can be observed that the traditional policy π_b 's input and output dimensions, which process the UCM and DCM vectors, scale with the total number of UEs. This generates an incompatibility with standard fixed-neuron architectures (e.g., multi-layer perceptron (MLP)), as any environment shift may invalidate the learned policy, forcing costly redesign and retraining from scratch. To address this kind of generalization challenge in dynamic environments, we take advantage of LLMs, which inherently process variable-length input and output sequences. Under this paradigm, fluctuations in the number of UEs merely alter the prompt's length rather than disrupting the fundamental training pipeline. Furthermore, the UCMs and DCMs evolve into interpretable semantic messages rather than opaque numerical values.

Specifically, we introduce a natural language vocabulary \mathcal{W}^2 and a mapping function set \mathcal{f} to adapt to the linguistic

¹As the policy π is a direct mapping from θ , updating the actor network's parameters constitutes an update to the policy itself.

²We assume both the BS and UEs utilize the same family of LLMs, thereby sharing \mathcal{W} .

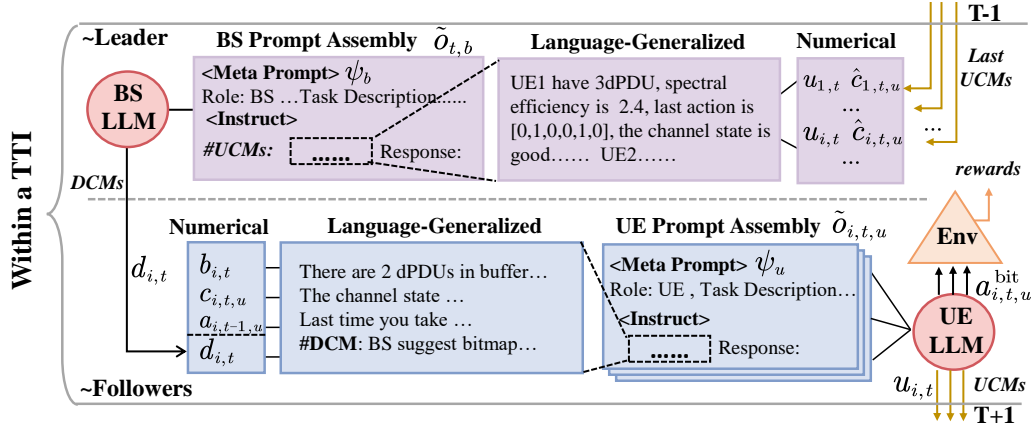


Fig. 2. The workflow of our LLM-powered MFSG within a TTI.

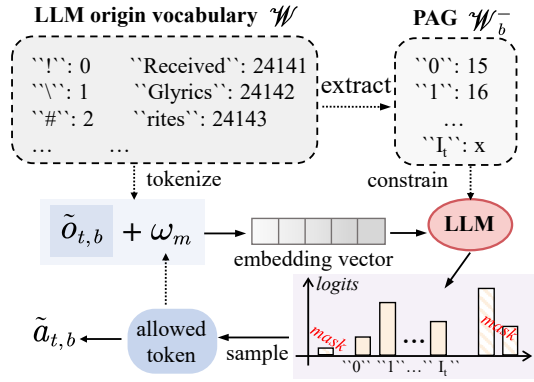


Fig. 3. LLM policy action generation with PAG.

modality. As depicted in Fig. 2, raw numerical observations $o_{t,b}, o_{i,t,u}$ are transformed into a comprehensive LLM-processable prompt through numeric-to-text conversion and meta-prompt assembly:

$$\tilde{o}_{i,t,u} \triangleq f_{o,u}(o_{i,t,u}) \oplus \psi_u, \tilde{o}_{i,t,u} \subset \mathcal{W} \quad (11a)$$

$$\tilde{o}_{t,b} \triangleq f_{o,b}(o_{t,b}) \oplus \psi_b, \tilde{o}_{t,b} \subset \mathcal{W}, \quad (11b)$$

where the tilde notation distinguishes the linguistic space from the primitive numerical space, $f_{o,u}, f_{o,b} \in \mathbf{f}$ convert the numerical observation vector into their linguistic representation, and ψ_u, ψ_b are meta-prompts containing natural language task descriptions and agent identity identifiers. The LLM then autoregressively generates a textual response that encapsulates the agent's action and signaling. Notably, this textual output must be parsed via an inverse mapping to be executed within the environment.

C. Generative Policy Architecture with PAG

LLMs' vast vocabulary and hallucination can produce responses containing irrelevant or unparseable tokens, which impairs the reliability. While default token filling is commonly used to maintain reliability [40], the sparsity of effective tokens remains a bottleneck in training efficiency. Therefore, we propose PAG to ensure the executability of the generated

responses, by constraining the output vocabulary to valid protocol-action tokens.

As depicted in Fig. 3, we construct the vocabulary space $\mathcal{W}_b^-, \mathcal{W}_u^- \subset \mathcal{W}$ that serves as the set of admissible protocol tokens for sampling. Precisely, the BS's output is constrained to only the numerical tokens within $\mathcal{W}_b^- = \{“0”, “1”, \dots, “I_t”\}$ that indicate the allocation of corresponding RBGs. Here, “0” indicates no allocation and others specify the allocation to the i -th UE. Each DCM action is then represented as a sequence $\tilde{a}_{t,b} = \{w_0, \dots, w_M\}$, $w \in \mathcal{W}_b^-$ of fixed length M , corresponding to the maximum number of allocable RBs. The probability of generating a specific, valid DCM is therefore calculated by

$$\mathbb{P}(\tilde{a}_{t,b} | \tilde{o}_{t,b}) = \prod_{j=0}^{|\tilde{a}_{t,b}|} \mathbb{P}(w_j | \tilde{o}_{t,b}, w_{<j}), \quad (12)$$

where $\mathbb{P}(w_j | \tilde{o}_{t,b}, w_{<j})$ represents the probability of generating token w_j given prompt $\tilde{o}_{t,b}$ and preceding tokens $w_{<j}$. To achieve computational efficiency, we obtain the log-probabilities from Eq. (12) and subsequently normalize these scores using a softmax function. This yields a policy distribution over the action space \mathcal{A}_b as

$$\pi_b(\tilde{a}_{t,b} | \tilde{o}_{t,b}) = \frac{\exp\{\sum_{j=0}^{|\tilde{a}_{t,b}|} \log \mathbb{P}(w_j | \tilde{o}_{t,b}, w_{<j})\}}{\sum_{\tilde{a}_{t,b} \in \mathcal{A}_b} \exp\{\sum_{j=0}^{|\tilde{a}_{t,b}|} \log \mathbb{P}(w_j | \tilde{o}_{t,b}, w_{<j})\}}. \quad (13)$$

Similarly, we can specify $\mathcal{W}_u^- = \{“0”, “1”\}$ to cater to the UE' action $a_{i,t,u}^{\text{bit}}$ and derive the UE policy $\pi_{i,u}$. Such policy formulation fully exploits the LLM's pre-trained generative priors to score the plausibility of actions, thereby obviating the need for auxiliary, randomly initialized output layers. It is thus robust to diverse action spaces without necessitating architectural modifications.

D. PPO-driven Functional Alignment and Adaptation

The training mechanism follows the principles from Section IV-A, but we tailor it substantially to accommodate the unique hierarchical structure of our dynamic MFSG. We instantiate LLM-powered actor (θ_b, θ_u) for BS and UEs, respectively, where dynamic UEs utilize the same neural network by parameter sharing. Their corresponding critic networks are

Algorithm 1 PPO Alignment of LLM-Agents for Protocol Emergence in Dynamic MFSG

Input: Discount factor γ and λ , learning rate α and β , time duration of each episode T .

- 1: Initialize (θ_b, ϕ_b) and (θ_u, ϕ_u) .
- 2: Initialize empty trajectory buffers \mathcal{B}_b for leader and \mathcal{B}_u for followers, respectively.
- 3: **while** epoch $e \leq e^{\max}$ **do**
- 4: Reset the UDTS environment and get initial observations $\tilde{o}_{0,b}, \{\tilde{o}_{i,0,u}\}_{i \in \mathcal{I}_t}$.
- 5: **for** each time slot $t \in \{0, 1, \dots, T\}$ **do**
- 6: // Coupled experience generation within a time slot
- 7: Leader (BS) selects action $\tilde{a}_{t,b} \sim \pi_b(\cdot | \tilde{o}_{t,b}; \theta_b)$ that determines the DCM. \triangleright Leader acts first
- 8: Each follower (UE i) observes local state and the DCM received from BS, selects action $\tilde{a}_{i,t,u} \sim \pi_u(\cdot | \tilde{o}_{i,t,u}; \theta_u)$, comprising the transmission bitmap and the UCM. \triangleright Followers react
- 9: Environment executes physical transmission actions $\{\tilde{\mathbf{a}}_{i,t,u}^{\text{bit}}\}_{i \in \mathcal{I}_t}$.
- 10: Environment returns the individual rewards $F_{t,b}, \{F_{i,t,u}\}_{i \in \mathcal{I}_t}$ and next observations. $\triangleright \tilde{o}_{t+1,b}$ now contains the UCMs $\{\tilde{u}_{i,t}\}_{i \in \mathcal{I}_t}$
- 11: **end for**
- 12: Store the trajectory rollout τ_b into buffer \mathcal{B}_b .
- 13: Aggregate the trajectory rollout from all UEs $\bigcup_{i \in \mathcal{I}_t} \tau_{i,u}$, and store into buffer \mathcal{B}_u .
- 14: // Independent policy updates
- 15: **for all** the leader and the followers **do**
- 16: **if** $|\mathcal{B}| \geq \text{Buffer Size}$ **then**
- 17: Minimize its critic's loss as detailed in Eq. (9).
- 18: Calculate the sampled policy gradient of Eq. (10).
- 19: Actor update $\theta^{(e+1)} \leftarrow \theta^{(e)} + \alpha \cdot \nabla J(\theta^{(e)})$.
- 20: Critic update $\phi^{(e+1)} \leftarrow \phi^{(e)} - \beta \cdot \nabla L(\phi^{(e)})$.
- 21: Clear experience buffer \mathcal{B} .
- 22: **end if**
- 23: **end for**
- 24: **end while**

realized by replacing the final layer of the initial LLM decoder block with a single-value head MLP. The training procedure, delineated in Algorithm 1, is orchestrated around the hierarchical experience coupling. Specifically, after an initial environment reset (line 5), the process unfolds within each TTI to precisely capture the game's sequential dependencies. The leader BS first executes its action $a_{t,b}$ (line 7), which consequently alters the observational space for all followers UEs. The followers then react based on this updated context (line 8), and their joint actions collectively determine the subsequent observations and rewards (lines 9–10). Although the trajectory data collected from this process is inherently coupled by the hierarchical interaction (lines 12–13), the leader and followers independently update their respective policy and value networks (lines 16–21). This process enables the policies to progressively align with the environment dynamics by grounding each update in causally correct, interdependent experiences.

E. Proof of Convergence

The co-adaptation of leader and follower policies in our dynamic MFSG creates an inherently non-stationary learning dynamic. This section therefore provides a formal proof that the gradient-based PPO alignment guides the framework to an equilibrium. We begin with fundamental assumptions and definitions.

Definition 1 (Expected Stackelberg Equilibrium [ESE]). *Let Θ_b and $\Theta_u = \Theta_{1,u} \times \dots \times \Theta_{I_t,u}$ be the policy parameter sets of BS and all UEs, respectively. A policy profile (θ_b^*, θ_u^*) is a dynamic follower ESE if the followers' policy θ_u^* constitutes an expected NE $h(\theta_b^*)$ in response to θ_b^* , where*

$$h(\theta_b^*) = \{ \theta_u^* \in \Theta_u \mid J_{i,u}(\theta_u^*, \theta_b) \geq J_{i,u}(\theta_{i,u}, \theta_{-i,u}^*, \theta_b^*), \forall i \}, \quad (14)$$

And the leader's policy maximizes its expected utility, anticipating the followers' best response from $h(\theta_b^*)$:

$$\theta_b^* \in \arg \max_{\theta_b \in \Theta_b} \inf_{\theta_u \in h(\theta_b)} J_b(\theta_b, \theta_u). \quad (15)$$

Consistent with standard practice in learning-in-games [41], [42], we only focus on local properties of the equilibrium and thus DSE is adopted.

Definition 2 (Differential Stackelberg Equilibrium [DSE] [42]). *A policy profile $\Theta^* = (\theta_b^*, \theta_u^*)$ constitutes a DSE, characterized by the following first- and second-order properties:*

- a) For UEs, θ_u^* satisfies the differential Nash equilibrium (DNE) condition [43], expressed as $\nabla_{\theta_{i,u}} J_{i,u}(\theta_b^*, \theta_u^*) = 0$ and $\nabla_{\theta_{i,u}}^2 J_{i,u}(\theta_b^*, \theta_u^*) \prec 0$;
- b) For BS, θ_b^* satisfies $\nabla_{\theta_b} \tilde{J}_b(\theta_b^*, h(\theta_b^*)) = 0$ and $\nabla_{\theta_b}^2 \tilde{J}_b(\theta_b^*, h(\theta_b^*)) \prec 0$, where $h(\theta_b^*)$ is the UEs' NE response.

To analyze the convergence of our PPO-based alignment, we also define the following policy update dynamics [42], [44].

Definition 3 (Policy Update Dynamics). *Let the joint policy parameters be denoted by the vector $\Theta = (\theta_b, \theta_u)^\top$. The learning process constitutes a discrete-time dynamical system governed by the update rule*

$$\Theta^{(e+1)} = \Theta^{(e)} + \alpha_b \cdot \Omega(\Theta^{(e)}), \quad (16)$$

where $\Omega(\Theta^{(e)}) = (\nabla_{\theta_b} J_b^{(e)}, \iota_u \nabla_{\theta_u} J_{1,u}^{(e)}, \dots, \iota_u \nabla_{\theta_u} J_{I_t,u}^{(e)})^\top$ is the update gradient vector, ι_u denotes the time scale separation factor³ and $\alpha_b \iota_u = \alpha_u$.

Furthermore, we make the following assumptions.

Assumption 1. *The policy parameter spaces Θ_b and Θ_u are non-empty compact sets. And the agents' utility functions, J_b and $J_{i,u}$ are sufficiently smooth, i.e, $J_b, J_{i,u} \in C^2(\Theta, \mathbb{R})$.*

This is a generic condition for gradient-based learning with neural network policies [45].

Assumption 2. *MFSG exhibits weak coupling near an equilibrium Θ^* , implying the second-order inter-player effects within*

³We assume all followers (UEs) adopt an identical time scale separation factor ι_u for simplicity.

their utility functions are negligible. That is, for any distinct agents $i, j, k \in \{b, u_1, \dots, u_{I_t}\}$,

$$\|\nabla_{\theta_i}^2 J_k(\Theta^*)\| \gg \|\nabla_{\theta_i, \theta_j} J_k(\Theta^*)\| \approx 0 \quad (17)$$

This is a reasonable simplification because an agent's utility gradient is predominantly influenced by its own policy parameters, particularly as interactions are mediated via an aggregate environment state.

To ensure that the protocol emergence process has a well-defined and reachable target, we begin by formally defining and proving the existence of such an equilibrium within our system. This result is formalized as Theorem 1.

Theorem 1 (Existence Theorem). *In our LLM-driven MFSG system – where BS acts as the leader and a dynamic number of UEs act as followers – an ESE policy profile (θ_b^*, θ_u^*) is guaranteed to exist.*

As completely proven in Appendix A, we analyze the equilibrium hierarchically. First, we show that the follower subgame is a potential game [46]. Hence, for any I_t , it admits an NE, i.e., the followers' best-response correspondence is nonempty. Next, in the dynamic-follower setting, we invoke Weierstrass' Theorem [47] to establish the existence of a solution to the leader's problem. Together, these results imply the existence of an ESE.

Based on the existence of equilibrium, we present a general convergence theorem, which states that the policy gradient update converges in a fixed-number MFSG.

Theorem 2 (Converge Theorem). *For the policy update dynamics described in the Definition 3, and under Assumptions 1 and 2, there exist positive constants κ_1, κ_2 such that if the leader's learning rate is set to $\alpha_b = \frac{\kappa_1}{\kappa_2}$, the sequence of policy parameters $\{\Theta^{(e)}\}_{e \geq 0}$ is guaranteed to converge locally to a DSE at a rate of $O\left(\left(1 - \frac{\kappa_1}{\kappa_2}\right)^{\frac{e}{2}}\right)$.*

We leave the proof in Appendix B while providing a proof sketch here. The logic is to show that the update map, $\Lambda(\Theta) = \Theta + \alpha_b \Omega(\Theta)$, is a local contraction around the DSE fixed point Θ^* . The analysis hinges on the property, derived in the appendix from Assumptions 1-2, that the symmetric part of the gradient field's Jacobian, $M(\Theta^*) = \frac{1}{2}(\mathbf{J}_\Omega^\top + \mathbf{J}_\Omega)$, is negative definite ($M(\Theta^*) \prec 0$). This allows for the selection of a learning rate $\alpha_b = \kappa_1/\kappa_2$, where $\kappa_1 = \sigma_{\min}(-M(\Theta^*))$, $\kappa_2 = \sigma_{\max}(\mathbf{J}_\Omega^\top \mathbf{J}_\Omega)$ and σ denotes a singular value, which guarantees contraction by satisfying

$$\|I + \alpha_b \mathbf{J}_\Omega(\Theta^*)\|_2^2 \leq 1 - \kappa_1^2/\kappa_2 < 1. \quad (18)$$

This result confirms that the spectral radius $\rho(\nabla \Lambda(\Theta^*)) < 1$, proving that Λ is a contraction and thus implying local geometric convergence to the DSE at the claimed rate.

In our dynamic MFSG setting, where the number of followers changes stochastically and all followers share a common LLM policy, we derive the following corollary.

Corollary 1. *Suppose all agents employ LLM-empowered policies for dynamic MFSG. Let the leader's policy be denoted by θ_b , and let all followers share a common policy θ_u . Regardless of the changes in the number of followers, Algorithm 1*

maintains the almost sure convergence properties established in Theorem 2.

We leave the proof in Appendix D, which extends Theorem 2 by analyzing the averaged learning dynamics over the distribution of followers. The simulation results in Fig. 5 further demonstrate that convergence is not only theoretically possible but also achievable in practice.

F. Complexity Analysis

The computational complexity of our framework is analyzed in terms of time, measured by floating point operations (FLOPs), and space, determined by network parameters. This complexity is jointly dictated by the LLM architecture – defined with n layers, a hidden dimension d_{model} , and feed-forward dimension d_{ffn} – and the hierarchical dynamics of the MFSG. The FLOPs for a single forward pass through the shared LLM backbone for a sequence of length ℓ is

$$\text{FLOPs}_f \approx O(n\ell^2 d_{\text{model}} + n\ell d_{\text{model}} d_{\text{ffn}}) \approx O(n\ell^2 d_{\text{model}}), \quad (19)$$

where the quadratic term originates from self-attention. This scaling is intrinsically asymmetric. For the leader, the prompt length is a function of I_t , i.e.,

$$\ell_{t,b} \approx \ell_{\psi_b} + \sum_{i=1}^{I_t} \ell_{i,u} \triangleq O(I_t), \quad (20)$$

where ℓ_{ψ_b} is the constant length of the meta-prompt and $\ell_{i,u}$ is the length of the tokenized UCM from UE followers. While the UE sequence length is constant $\ell_{i,u} = O(1)$. Consequently, the leader's actor network, which autoregressively generates a fixed-length action sequence of M tokens, results in a cost of $O(M \cdot I_t^2 \cdot n d_{\text{model}})$. The critic network requires a single forward pass of cost $O(I_t^2 \cdot n d_{\text{model}})$. On the other hand, for all I_t followers, the aggregate cost is $O(M \cdot I_t \cdot n d_{\text{model}})$. With I_t varying over time according to a distribution, the total training complexity over e^{\max} epochs is best characterized by its expected value

$$O\left(e^{\max} T \cdot M n d_{\text{model}} (\mathbb{E}[I_t^2] + \mathbb{E}[I_t])\right). \quad (21)$$

In contrast, the per-decision inference cost is an instantaneous measure dependent on the current I_t , given by the sum of the leader's and followers' forward generation costs $O(M I_t^2 n d_{\text{model}} + I_t M n d_{\text{model}})$.

The total space complexity during training is the sum of storage for all network parameters and experience replay buffers, totaling $O(n d_{\text{model}}^2 + |\mathcal{B}_b| + |\mathcal{B}_u|)$. During inference, this requirement reduces to storing only the actor network parameters, yielding a space complexity of $O(n d_{\text{model}}^2)$.

V. SIMULATION RESULTS

In this section, we first detail the simulation setup and the baseline methods. We then compare the performance of our proposed framework against the baselines under various scenarios. Additionally, we include ablation studies and hyperparameter sensitivity analysis.

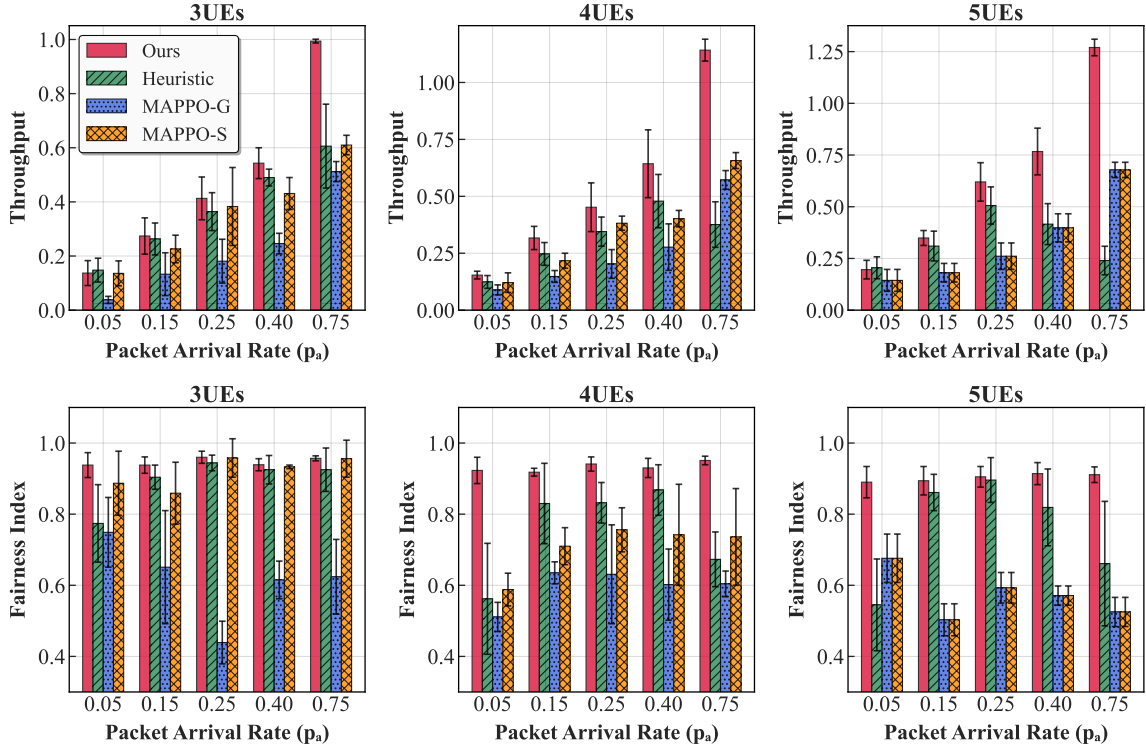


Fig. 4. Performance comparison of throughput and fairness index under various packet arrival rates and network sizes, where p_a of all UEs is set to the same value for each case.

TABLE III
SIMULATION PARAMETERS.

Parameter	Symbol	Value
Number of UEs	I	$\{3, 4, 5\}$
Transport block size (bit)	ξ^{gen}	256
Buffer capacity of each UE	B_{cap}	∞
TTI duration	TTI	5×10^{-3} s
The arrive rate of dPDU	p_a	$[0.05, 0.75]$
Number of RBGs	M	5
Discount factor	γ, λ	0.95, 0.9
Transport block error rate	TBLER	10^{-3}
Clipping parameter of PPO	ϵ	0.1
Learning rate	α, β	$5 \times 10^{-4}, 1 \times 10^{-5}$
Numerology parameters	$N_{\text{sc}}^{\text{rb}}, N_{\text{symbol}}^{\text{sh}}$	12, 14
Total training epochs	e^{max}	2000
Weighting parameter	$\rho_1, \rho_2, \varepsilon$	8, 10, 5
Channel changing frequency		$[1, 10]$ ms
Actor temperature range		$[0.3, 3]$
PPO update epochs		5
Mini-batch size		128

A. Simulation Setup

We consider a UDTs environment where the number of UEs I_t varies within the set $\{3, 4, 5\}$. Each episode spans $T = 24$ TTIs, with a TTI duration of 5×10^{-3} s. UEs commence with an empty and sufficiently large buffer to prevent overflow. By default, three distinct $p_a \in \{0.1, 0.3, 0.7\}$ are assigned to UEs cyclically to model heterogeneous traffic loads, with a fixed dPDU size $\xi^{\text{gen}} = 256$ bits. Each UE's channel transitions between “poor”, “medium”, and “good” states with a changing frequency in $[1, 10]$ ms, where each state maps to a spectral

efficiency $\nu_{i,t}$ via a pre-defined MCS lookup table. Moreover, we set $N_{\text{sc}}^{\text{rb}} = 12$, $N_{\text{symbol}}^{\text{sh}} = 14$, aligning with the commonly deployed 3GPP new radio (NR) configuration [36], [37].

We employ open-source Llama3-1B [48] as the actor-critic backbone. The critic network is augmented with a three-layer value head (1024 hidden neurons per layer and ReLU activations) to produce scalar state values. The actor's temperature linearly decays from 3.0 to 0.3 during training. To facilitate online training, we perform 5 epochs of PPO updates after collecting 10 full episodes, after which the buffer \mathcal{B} is cleared for new collections. The PPO updates utilize a mini-batch size of 128, an Adam optimizer with a learning rate of 5×10^{-4} , and a cosine learning rate decay schedule. We totally train for 3000 epochs, periodically evaluating the learned protocol's performance in fixed-UE settings over five independent runs. Experiments are conducted on a server running Ubuntu 22.04.5, equipped with an AMD EPYC 7763 64-Core CPU, 1 TiB of RAM, and eight NVIDIA A800 GPUs. The software stack includes Python 3.12, CUDA 12.2, and PyTorch 2.5. A summary of the simulation parameters is provided in Table III. Furthermore, we consider the following baseline methods:

- **Heuristic**: An enhanced S-ALOHA [24] where each UE initially transmits a dPDU with a probability 0.5, which is then adaptively decreased upon a collision.
- **MAPPO-S**: Symbolic MAPPO algorithm for protocol emergence, as presented in [6], which is retrained for each specific scenario to adapt to environmental shifts.
- **MAPPO-G**: The same MAPPO architecture, but trained

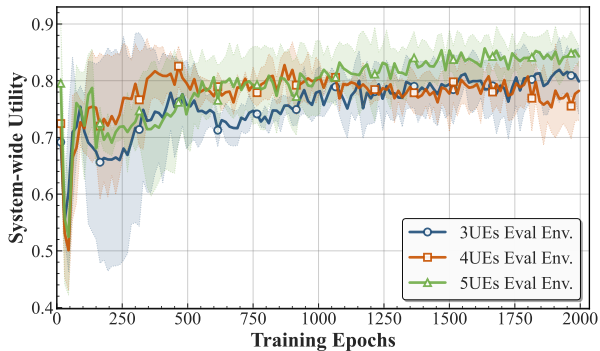


Fig. 5. Convergence of normalized system-wide utility during training in evaluation environments with varying UE numbers.

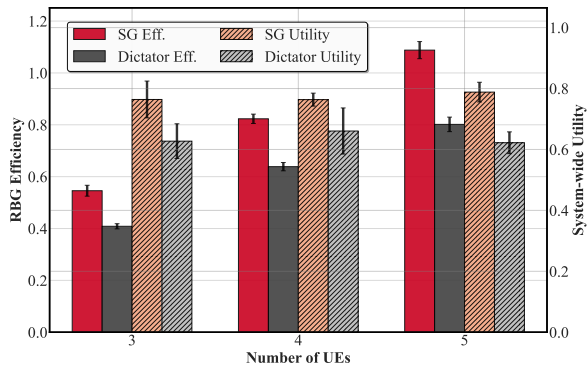


Fig. 6. Ablation study on the impact of the hierarchical SG mechanism.

in one scenario and directly applied to others without retraining to evaluate its generalization capabilities.

Finally, to compare the performance of different methods, we introduce the following network KPIs.

- 1) *Throughput*: We define the average throughput of our system as the number of dPDU bits received by BS per active UE per unit of time, computed over all TTIs by

$$\text{Th} = \frac{1}{T \cdot \text{TTI}} \sum_{t=1}^T \left(\frac{1}{|\mathcal{J}_t|} \sum_{i \in \mathcal{J}_t} \xi_{i,t,u}^{\text{rec}} \right). \quad (22)$$

- 2) *Fairness Index*: We utilize the Jain's Fairness Index [39] as detailed in the second term of Eq. (6).
- 3) *Resource Efficiency*: We introduce the Eff metric to evaluate the system's resource efficiency, defined as the received dPDUs divided by the total RBG utilization

$$\text{Eff} = \frac{\sum_{t=1}^T \sum_{i \in \mathcal{J}_t} \xi_{i,t,u}^{\text{rec}}}{\sum_{i \in \mathcal{J}_T} x_{i,T,u}}. \quad (23)$$

B. Numerical Results and Analysis

1) *Comparative Analysis with Baselines*: Fig. 4 presents a comparative evaluation of the proposed framework against baseline methods, highlighting average throughput and fairness across varying network sizes and arrival rates. In terms of the average throughput, i.e., the top row of Fig. 4, our proposed method consistently and substantially outperforms

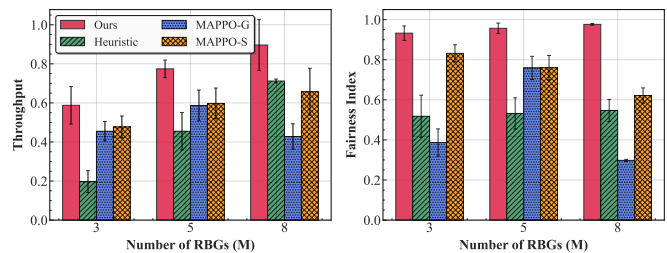


Fig. 7. Performance comparison of throughput and fairness index with a varying number of RBGs.

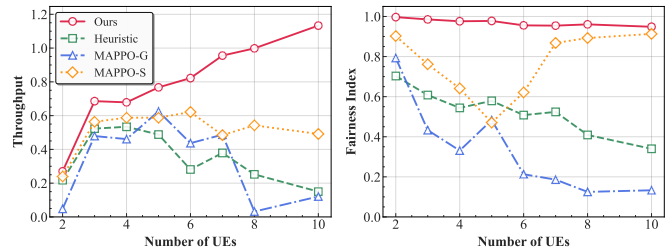


Fig. 8. Performance scalability with an increasing number of UEs.

all baselines across every tested configuration. Moreover, the framework's superiority is particularly pronounced in high-contention scenarios. For instance, with 5 UEs and a high arrival rate of $p_a = 0.75$, our approach achieves a throughput of approximately 1.27, marking a significant improvement of over 77.65% compared to the retrained MAPPO-S baseline and 212.43% over the generalized MAPPO-G. Our framework also achieves improvements of at least 24.68% compared with Heuristic baseline. Furthermore, the severe performance degradation of MAPPO-G validates the poor generalization capability of conventional MARL approaches, a critical limitation that LLM-empowered framework successfully addresses. In terms of the fairness index, as shown in the second row of Fig. 4, our framework maintains a near-optimal fairness index, consistently exceeding 0.9, ensuring equitable resource allocation among UEs. Specifically, the advantage of our framework is significant in the 4-UE scenario, delivering average throughput improvements of approximately 24.82%, 56.31%, and 32.02% over the Heuristic, MAPPO-G, and MAPPO-S baselines across all arrival rates. In the less congested 3-UE scenario, the performance gap is reduced, yet our method still provides notable gains of approximately 5.81%, 53.73%, and 3.14%, respectively. In stark contrast, the fairness index of both the Heuristic and MAPPO-G methods deteriorates sharply. It drops below 0.6 in the 5 UEs scenario, indicating their failure to resolve collisions and manage contention effectively. The consistently high performance across different network scales demonstrates our framework's strong generalization capability, operating on dynamic network topologies without the need for retraining.

Fig. 5 illustrates the convergence of the system-wide utility during the PPO training. The utility steadily improves and converges to approximately 0.8 across all evaluated scenarios after approximately 1,250 training epochs, empirically vali-

TABLE IV
THE IMPACT OF LLM MODEL SCALE AND VARIANT ON DIFFERENT PERFORMANCE METRICS.

Metrics	MAPPO	GPT2	Llama3-1B	Qwen3-4B
GPU Memory	576MiB	13.38GiB	44.76GiB	77.84GiB
JFI	0.8127	0.9709	0.9883	0.9576
Throughput	0.42	0.58	0.65	0.68
RBG Efficiency	0.31	0.49	0.53	0.52

dating the convergence guarantee established in Corollary 1.

2) *Contribution of SG Mechanism*: To validate the superiority of our proposed MFSG mechanism, we conduct an ablation study comparing its performance against a centralized "Dictator" scheme. In this baseline, UEs (followers) forfeit their autonomy, rigidly adhering to the BS's (leader's) scheduling commands without local optimization. As depicted in Fig. 6, the SG framework yields average gains of approximately 24.74% in RBG efficiency and 17.58% in system utility. This result highlights that the modeled leader-follower hierarchy effectively balances macroscopic coordination with the exploitation of local UE dynamics, resulting in superior resource utilization and overall system performance.

3) *Impact of Different RBGs*: Fig. 7 evaluates the framework's performance and adaptability when varying the number of RBGs while maintaining other parameters unchanged. The left chart indicates that increasing resource M enhances throughput to a certain degree. When M increases from 3 to 8, our method scales effectively with increased resource availability, with a further improvement of 39.41%. With $M = 8$ RBGs, our method achieves a throughput of approximately 0.9, surpassing the retrained MAPPO-S by around 38.75%. Most notably, MAPPO-G exhibits a critical failure in generalization – its throughput paradoxically decreases as more resources become available, dropping from 0.45 at $M = 3$ to 0.25 at $M = 8$. The fairness results on the right further highlight the robustness of our approach, which maintains a high fairness index regardless of the number of RBGs, ensuring equitable resource distribution. While MAPPO-S also maintains an adequate fairness index, it achieves approximately 29.82% lower performance compared to ours.

4) *Impact of Number of UEs*: Fig. 8 illustrates the framework's scalability as the number of competing UEs increases from 2 to 10. Throughput for our method scales approximately linearly, whereas competing approaches degrade in large-network scenarios. Crucially, these throughput gains are achieved with strong equity, as the fairness index remains above 0.95 across all network sizes. On average, our method achieves throughput gains of approximately 55.23%, 34.59%, and 57.37% over Heuristic, MAPPO-S, and MAPPO-G, respectively, while improving the fairness index by about 45.64%, 21.72%, and 65.22%. This result highlights a limitation of the conventional MARL and heuristic approaches, demonstrating that our LLM-empowered protocol is more adaptable to larger-scale and dynamic network conditions.

5) *Impact of Different LLMs*: Table IV analyzes both the performance and computational overheads across different model variants. The LLM-based models demonstrate superior

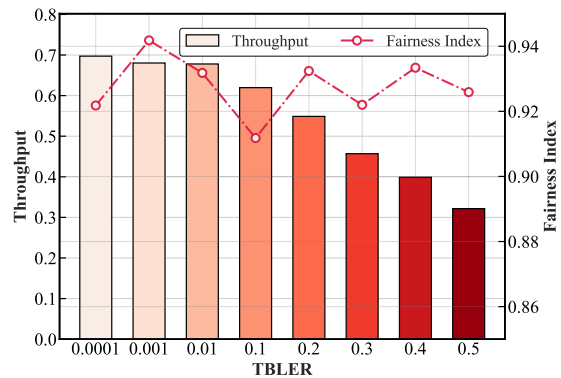


Fig. 9. Impact of TBLER on system throughput and fairness index.

network KPIs compared to the lightweight MAPPO baseline, albeit at the cost of higher resource utilization. Our selected Llama3-1B model, for instance, improves throughput by 54.76% and RBG efficiency by 70.96% over MAPPO. Smaller GPT2-small outperforms MAPPO with a moderate latency trade-off, while the largest Qwen3-4B model incurs prohibitive overhead for marginal performance gains compared to Llama3-1B.

6) *Impact of TBLER*: Fig. 9 assesses the robustness of the proposed framework under varying TBLER conditions. The results indicate that as the TBLER increases from 0.0001 to 0.5, the system throughput exhibits a smooth decline from approximately 0.7 to 0.32, in line with theoretical expectations. Notably, even under severe channel degradation where throughput is nearly halved, the fairness index consistently remains above 0.92, thereby substantiating the robustness of the learned MAC protocol.

VI. CONCLUSION

In this paper, we have focused on the critical challenge of autonomously establishing generalizable and adaptive MAC protocols for dynamic wireless networks, where traditional MARL methods require costly retraining and redesign. We have proposed a novel LLM-empowered framework that recasts protocol emergence as a dynamic MFSG, capturing the intrinsic hierarchical interactions among network agents. By employing LLMs as policy networks within a PPO-driven RL loop, the framework natively handled variable-length inputs and outputs while preserving the exploratory learning required for protocol discovery. Theoretical analyses have guaranteed the existence of equilibria and the convergence of the proposed method. Simulation results have demonstrated that our method can robustly adapt to dynamic network conditions and consistently outperform various heuristic and conventional MAPPO baselines across diverse KPIs and environmental settings. A promising direction for future work is to extend this game-theoretic, LLM-based MAC protocol to more complex scenarios, such as multi-cell deployments and integrated sensing and communication protocols.

REFERENCES

- [1] M. Bennis, "Resilient-native and intelligent nextG systems," 2025. [Online]. Available: <https://arxiv.org/abs/2506.12795>

- [2] M. Han, X. Sun, X. Wang, *et al.*, “Foundation model enhanced multiple access in heterogeneous networks,” *IEEE Trans. Mobile Comput.*, vol. 24, no. 9, pp. 8974–8987, Sep. 2025.
- [3] A. Valcarce and J. Hoydis, “Toward joint learning of optimal MAC signaling and wireless channel access,” *IEEE Trans. Cognit. Commun. Netw.*, vol. 7, no. 4, pp. 1233–1243, Oct. 2021.
- [4] M. P. Mota, A. Valcarce, J.-M. Gorce, *et al.*, “The emergence of wireless MAC protocols with multi-agent reinforcement learning,” in *Proc. IEEE Global Commun. Conf.*, Madrid, Spain, Dec. 2021.
- [5] M. P. Mota, A. Valcarce, and J.-M. Gorce, “Scalable joint learning of wireless multiple-access policies and their signaling,” in *Proc. IEEE Veh. Technol. Conf.*, Helsinki, Finland, Jun. 2022.
- [6] S. Mostafa, M. P. Mota, A. Valcarce, *et al.*, “Intent-aware DRL-based NOMA uplink dynamic scheduler for IIoT,” 2025. [Online]. Available: <https://arxiv.org/abs/2403.18364>
- [7] A. Pastore, A. A. de Dios, and Álvaro Valcarce, “Optimizing wireless discontinuous reception via MAC signaling learning,” 2024. [Online]. Available: <https://arxiv.org/abs/2406.13834>
- [8] L. Miuccio, S. Riolo, S. Samarakoon, *et al.*, “On learning generalized wireless MAC communication protocols via a feasible multi-agent reinforcement learning framework,” *IEEE Trans. Mach. Learn. Commun. Networking*, vol. 2, pp. 298–317, Feb. 2024.
- [9] M. A. Jadoon, A. Pastore, M. Navarro, *et al.*, “Learning random access schemes for massive machine-type communication with marl,” *IEEE Trans. Mach. Learn. Commun. Netw.*, vol. 2, pp. 95–109, Oct. 2024.
- [10] R. Tan, R. Li, and Z. Zhao, “LLM4MAC: An LLM-driven reinforcement learning framework for MAC protocol emergence,” in *Proc. IEEE SPAWC*, Surrey, UK, Jul. 2025.
- [11] B. Huang and A. Guo, “A dynamic hierarchical game approach for user association and resource allocation in hetnets with wireless backhaul,” *IEEE Wirel. Commun. Lett.*, vol. 13, no. 1, pp. 59–63, Jan. 2024.
- [12] D. Shi, L. Li, T. Ohtsuki, *et al.*, “Make smart decisions faster: Deciding D2D resource allocation via Stackelberg game guided multi-agent deep reinforcement learning,” *IEEE Trans. Mobile Comput.*, vol. 21, no. 12, pp. 4426–4438, Dec. 2022.
- [13] J. Park, S.-W. Ko, J. Choi, *et al.*, “Towards semantic communication protocols for 6G: From protocol learning to language-oriented approaches,” 2023. [Online]. Available: <https://arxiv.org/abs/2310.09506>
- [14] B. Liu, Y. Lu, J. Zhao, *et al.*, “WiLLM: an open framework for LLM services over wireless systems,” 2025. [Online]. Available: <https://arxiv.org/abs/2506.19030>
- [15] L. Liang, H. Ye, Y. Sheng, *et al.*, “Large language models for wireless communications: From adaptation to autonomy,” 2025. [Online]. Available: <https://arxiv.org/abs/2507.21524>
- [16] T. Carta, C. Romac, T. Wolf, *et al.*, “Grounding large language models in interactive environments with online reinforcement learning,” in *Proc. Int. Conf. Mach. Learn.*, Honolulu, Hawaii, USA, Jul. 2023, p. 3676–3713.
- [17] S. Sarbu, M. P. Mota, and M. Bennis, “On scaling latency-aware MAC communication protocols with a hierarchical network topology,” in *Proc. IEEE Int. Conf. Commun.*, Denver, CO, USA, Jun. 2024, pp. 2555–2560.
- [18] A. Sheth, I. Sheth, and M. Fritz, “ProtocolLLM: RTL benchmark for systemverilog generation of communication protocols,” 2025. [Online]. Available: <https://arxiv.org/abs/2506.07945>
- [19] Z. Liu, B. Liu, A. Valcarce, *et al.*, “LLM-based emulation of the radio resource control layer: Towards AI-native RAN protocols,” 2025. [Online]. Available: <https://arxiv.org/abs/2505.16821>
- [20] Z. Chen, X. Sun, Y. Jin, *et al.*, “Multi-task reinforcement learning-based multiple access for dynamic wireless networks,” *IEEE Trans. Mobile Comput.*, vol. 24, no. 9, pp. 9153–9167, Sep. 2025.
- [21] Y. Kim, S. Seo, J. Park, *et al.*, “Knowledge distillation from language-oriented to emergent communication for multi-agent remote control,” in *Proc. IEEE Int. Conf. Commun.*, vol. 23, no. 7, Denver, CO, USA, Jun. 2024, pp. 7000–7012.
- [22] S. Seo, J. Park, S.-W. Ko, *et al.*, “Toward semantic communication protocols: A probabilistic logic perspective,” *IEEE J. Sel. Areas Commun.*, vol. 41, no. 8, pp. 2670–2686, Aug. 2023.
- [23] D. C. Kwon and X. Zhang, “CP-AgentNet: Autonomous and explainable communication protocol design using generative agents,” 2025. [Online]. Available: <https://arxiv.org/abs/2503.17850>
- [24] Y. Kim, J. Park, M. Bennis, *et al.*, “Resilient LLM-empowered semantic MAC protocols via zero-shot adaptation and knowledge distillation,” 2025. [Online]. Available: <https://arxiv.org/abs/2505.21518>
- [25] N. Keshtiarast and M. Petrova, “ML framework for wireless MAC protocol design,” in *Proc. IEEE Int. Conf. Mach. Learn. Commun. Netw.*, Stockholm, Sweden, May 2024, pp. 560–565.
- [26] N. Keshtiarast, O. Renaldi, and M. Petrova, “Wireless MAC protocol synthesis and optimization with multi-agent distributed reinforcement learning,” *IEEE Netw. Lett.*, vol. 6, no. 4, pp. 242–246, Dec. 2024.
- [27] K. Szczech, M. Wojnar, K. Kosek-Szott, *et al.*, “Toward specialized wireless networks using an ML-driven radio interface,” *IEEE Access*, vol. 13, pp. 141 814–141 831, Aug. 2025.
- [28] Z. Guo, Z. Chen, P. Liu, *et al.*, “Multi-agent reinforcement learning-based distributed channel access for next generation wireless networks,” *IEEE J. Sel. Areas Commun.*, vol. 40, no. 5, pp. 1587–1599, May 2022.
- [29] Y. Chen, R. Li, Z. Zhao, *et al.*, “NetGPT: An AI-native network architecture for provisioning beyond personalized generative services,” *IEEE Network*, vol. 38, no. 6, pp. 404–413, Nov. 2024.
- [30] W. Lee and J. Park, “LLM-empowered resource allocation in wireless communications systems,” 2024. [Online]. Available: <https://arxiv.org/abs/2408.02944>
- [31] J. Shao, J. Tong, Q. Wu, *et al.*, “WirelessLLM: Empowering large language models towards wireless intelligence,” *IEEE J. Commun. Info. Netw.*, vol. 9, no. 2, pp. 99–112, Jun. 2024.
- [32] T. D. Tran and L. B. Le, “Resource allocation for multi-tenant network slicing: A multi-leader multi-follower Stackelberg game approach,” *IEEE Trans. Veh. Technol.*, vol. 69, no. 8, pp. 8886–8899, Aug. 2020.
- [33] L. Zhai, Y. Zou, J. Zhu, *et al.*, “A Stackelberg game approach for IRS-aided WPCN multicast systems,” *IEEE Trans. Wireles Commun.*, vol. 21, no. 5, pp. 3249–3262, May 2022.
- [34] T. Lyu, H. Xu, F. Liu, *et al.*, “Two layer Stackelberg game-based resource allocation in cloud-network convergence service computing,” *IEEE Trans. Cognit. Commun. Netw.*, vol. 10, no. 6, pp. 2412–2426, Dec. 2024.
- [35] Y. Geng, E. Liu, W. Ni, *et al.*, “Balancing performance and cost for two-hop cooperative communications: Stackelberg game and distributed multi-agent reinforcement learning,” *IEEE Trans. Cognit. Commun. Netw.*, vol. 10, no. 6, pp. 2193–2208, Dec. 2024.
- [36] 3GPP, “3rd generation partnership project; technical specification group radio access network; NR; medium access control (MAC) protocol specification (release 18),” 3GPP, Tech. Rep. TS 38.321 V18.6.0, 2025.
- [37] 3GPP, “3rd generation partnership project; technical specification group radio access network; NR; physical layer procedures for data (release 18),” 3GPP, Tech. Rep. TS 38.214 V18.7.0, 2025.
- [38] J. Wang, H. T. Shen, J. Song, *et al.*, “Hashing for similarity search: A survey,” 2014.
- [39] R. Jain, D. Chiu, and W. Hawe, “A quantitative measure of fairness and discrimination for resource allocation in shared computer systems,” 1998. [Online]. Available: <https://arxiv.org/abs/cs/9809099>
- [40] Y. Xiang, S. Li, R. Li, *et al.*, “Decentralized consensus inference-based hierarchical reinforcement learning for multiconstrained UAV pursuit-evasion game,” *IEEE Trans. Neural Netw. Learn. Syst.*, 2025, early access.
- [41] L. Zheng, T. Fiez, Z. Alumbaugh, *et al.*, “Stackelberg actor-critic: Game-theoretic reinforcement learning algorithms,” *AAAI Conf. Artif. Intell.*, vol. 36, no. 8, pp. 9217–9224, Jun. 2022.
- [42] T. Fiez, B. Chasnov, and L. Ratliff, “Implicit learning dynamics in Stackelberg games: equilibria characterization, convergence analysis, and empirical study,” in *Proc. Int. Conf. Mach. Learn.*, Virtual Edition, Jul. 2020, p. 3133–3144.
- [43] L. J. Ratliff, S. A. Burden, and S. S. Sastry, “On the characterization of local Nash equilibria in continuous games,” *IEEE Trans. Autom. Contr.*, vol. 61, no. 8, pp. 2301–2307, Jun. 2016.
- [44] F. Morri, H. L. Cadre, and L. Brotcorne, “Learning in conjectural Stackelberg games,” 2025. [Online]. Available: <https://arxiv.org/abs/2501.13686>
- [45] V. Konda and J. Tsitsiklis, “Actor-critic algorithms,” *Adv. Neural Inf. Process. Syst.*, p. 1008–1014, 1999.
- [46] J. Chen, Q. Wu, Y. Xu, *et al.*, “Joint task assignment and spectrum allocation in heterogeneous UAV communication networks: A coalition formation game-theoretic approach,” *IEEE Trans. Wirel. Commun.*, vol. 20, no. 1, pp. 440–452, Jan. 2021.
- [47] N. Cotter, “The Stone-Weierstrass theorem and its application to neural networks,” *IEEE Trans. Neural Networks*, vol. 1, no. 4, pp. 290–295, Dec. 1990.
- [48] A. Grattafiori, A. Dubey, A. Jauhri, *et al.*, “The Llama 3 herd of models,” 2024. [Online]. Available: <https://arxiv.org/abs/2407.21783>
- [49] F. Sun, Y. Li, Y. Wen, *et al.*, “Multi-agent feedback enabled neural networks for intelligent communications,” *IEEE Trans. Wirel. Commun.*, vol. 21, no. 8, pp. 6167–6179, Feb. 2022.
- [50] M. L. Puterman, “Markov decision processes,” in *Stochastic Models*, ser. Handbooks in Operations Research and Management Science. Elsevier, 1990, vol. 2, pp. 331–434.

- [51] A. Granas, J. Dugundji, *et al.*, *Fixed point theory*. Springer, 2003, vol. 14.
- [52] J. M. Ortega and W. C. Rheinboldt, *Iterative solution of nonlinear equations in several variables*. SIAM, 2000.
- [53] R. A. Horn and F. Zhang, "Basic properties of the Schur complement," in *The Schur complement and its applications*. Springer, 2005, pp. 17–46.
- [54] R. A. Horn and C. R. Johnson, *Topics in matrix analysis*. Cambridge University Press, 1994.

APPENDIX A
PROOF OF THEOREM 1

For ease of reference, we first present a table summarizing the notations used throughout the proofs as Table V. To establish the existence of an ESE, we first introduce two foundational lemmas.

Lemma 1 (Weierstrass Theorem [47]). *A continuous function defined on a non-empty, compact set is guaranteed to attain its maximum and minimum values on that set.*

Lemma 2 (Implicit Function Theorem [49]). *Given a system $\mathcal{G}(\mathbf{x}, \mathbf{y}) = 0$, if the Jacobian matrix of \mathcal{G} with respect to \mathbf{y} , denoted by $\mathbf{J}_{\mathcal{G}}$, is non-singular at a point (\mathbf{x}, \mathbf{y}) that satisfy the system, then there exist a unique, continuously differentiable function $h(\mathbf{x})$ in a neighborhood of \mathbf{y} such that $\mathcal{G}(\mathbf{x}, h(\mathbf{x})) = 0$.*

The mind map of the proof is illustrated in Fig. 10. Inspired by backward induction, we hierarchically analyze the MFSG. We first prove the existence of NE in a multi-follower subgame with any follower numbers, and then establish the existence of a solution for the leader's problem.

A. Existence of NE in Follower Subgame

Consider the subgame among followers under any fixed leader policy θ_b and any realized number of followers $\mathcal{I}_t = I$ drawn from the distribution $\mathbb{D}(I)$. We next show that this subgame is an exact potential game (EPG), which admits at least one NE [46]. First, we focus on the interactive term $\xi_{i,t,u}^{\text{rec}}/\xi_{i,t,u}^{\text{tx}}$ from Eq. (2), since the other term is independent

TABLE V
NOTATIONS USED IN APPENDIX.

Notation	Description
θ_b, θ_u	Specific policy parameters for the leader and followers
$\Theta^{(e)}, \Theta^*$	Joint policy parameters at epoch e and equilibrium point, respectively
$J_b(\cdot), J_{i,u}(\cdot)$	The expected long-term utility functions for the leader and follower u_i
$h(\theta_b)$	The best-response of followers given the leader's policy θ_b
$F'_{i,t,u}$	The interactive term in the follower's utility function, dependent on other followers' actions
\mathbf{a}^{bit}	The joint transmission bitmaps $a_{i,t,u}^{\text{bit}}$ of all followers
$\mathcal{E}(\cdot)$	The potential function for follower subgame
$\Omega(\cdot)$	The update gradient field for policy parameters
$\Xi_m(\cdot)$	The number of UEs selecting RBG m
$\mathcal{C}_m(\cdot)$	Payoff function at RBG m
N_m	The transmitted data volume at RBG m
$\mathcal{G}(\theta_b, h(\theta_b))$	The system of first-order conditions defining the followers' DNE given the leader's policy θ_b
$\Lambda(\Theta)$	The map of the discrete-time dynamical system governing the policy updates
$\sigma(\cdot)$	Singular value of a matrix
$\mathbf{J}_{\mathcal{G}}$	The Jacobian matrix of the FOC system $\mathcal{G}(\cdot)$
\mathbf{J}_{Ω}	The Jacobian matrix of the gradient field $\Omega(\cdot)$
$\mathbf{M}(\Theta)$	The symmetric part of the Jacobian matrix \mathbf{J}_{Ω}
κ_1, κ_2	Positive constants derived from the singular values of $\mathbf{M}(\Theta)$ and \mathbf{J}_{Ω} , related to the convergence rate
ι_u	The time-scale separation factor for the followers' learning relative to the leader's

Goal: Prove the existence of an Stackelberg Equilibrium
Strategy: Backward Induction

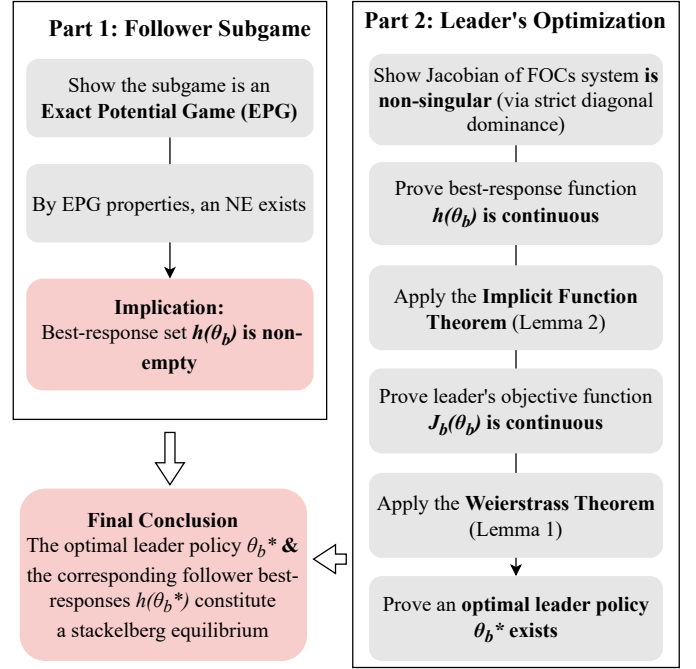


Fig. 10. Proof roadmap for existence theorem

of other follower actions. To construct the potential function, we then reformulate this interactive utility $F'_{i,t,u}$ as

$$F'_{i,t,u}(\mathbf{a}^{\text{bit}}; a_{t,b}, I) = \sum_{m=1}^M a_{i,t,u,m}^{\text{bit}} \left(\prod_{j \in \mathcal{I}_t, j \neq i} (1 - a_{j,t,u,m}^{\text{bit}}) N_m \right), \quad (24)$$

where $\mathbf{a}^{\text{bit}} = (a_{i,t,u}^{\text{bit}}, a_{-i,t,u}^{\text{bit}})$, $a_{i,t,u}^{\text{bit}} = (a_{i,t,u,1}^{\text{bit}}, \dots, a_{i,t,u,M}^{\text{bit}})$, and N_m denotes data transmitted⁴ on RBG m . Based on this, we can define an exact potential function that captures the network throughput for the joint action profile \mathbf{a}^{bit}

$$\mathcal{E}(\mathbf{a}^{\text{bit}}; a_{t,b}, I) = \sum_{m=1}^M \sum_{j=1}^{\Xi_m(\mathbf{a}^{\text{bit}})} \mathcal{C}_m(j), \quad (25)$$

where $\Xi_m(\mathbf{a})$ is the number of UEs selecting RBG m , and the payoff function $\mathcal{C}_m(x) = N_m$ if $x = 1$ and 0 otherwise. The proposed potential function has a corresponding physical meaning, which is equal to the network throughput. Accordingly, it can be easily shown that for any UE i and any unilateral change in its action from $a_{i,t,u}^{\text{bit}}$ to $\hat{a}_{i,t,u}^{\text{bit}}$,

$$\begin{aligned} & F'_{i,t,u}(\hat{a}_{i,t,u}^{\text{bit}}, a_{-i,t,u}^{\text{bit}}; a_{t,b}, I) - F'_{i,t,u}(a_{i,t,u}^{\text{bit}}, a_{-i,t,u}^{\text{bit}}; a_{t,b}, I) \\ &= \mathcal{E}(\hat{a}_{i,t,u}^{\text{bit}}, a_{-i,t,u}^{\text{bit}}; a_{t,b}, I) - \mathcal{E}(a_{i,t,u}^{\text{bit}}, a_{-i,t,u}^{\text{bit}}; a_{t,b}, I), \end{aligned} \quad (26)$$

confirming \mathcal{E} as an exact potential function. Therefore, for any leader policy θ_b and any finite number of followers I , there exists an NE among the follower subgame, which guarantees the set of followers' best-response policies $h(\theta_b)$ is nonempty.

⁴We assume all UEs share the common N_m for simplicity.

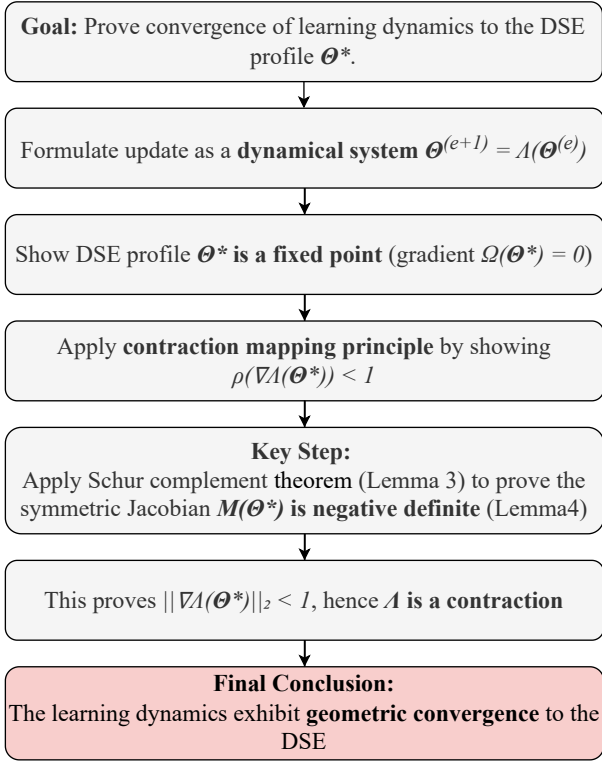


Fig. 11. Proof roadmap for convergence theorem.

B. Existence of an Optimal Universal Leader Policy

We next analyze the leader's problem as shown in Eq. (6), which can be reformulated as the parameterized value function form

$$\max_{\theta_b \in \Theta_b} J_b(\theta_b) = \mathbb{E}_{I \sim \mathbb{D}(I)} [V_b(\theta_b, h(\theta_b), I)], \quad (27)$$

where $V_b(\theta_b, h(\theta_b), I)$ is the long-term value function for a given instance I . By Lemma 1, we just need to justify the continuity of J_b , which can be established by demonstrating the continuity of the value function V_b for each I . The continuity of V_b , in turn, hinges on the continuity of the effective stage-game utility $F_{t,b}(\theta_b, h(\theta_b), I)$, which depends on the followers' best-response function $h(\theta_b)$.

Specifically, $h(\theta_b)$ is implicitly defined by the first-order conditions (FOCs) in Definition 2, i.e.,

$$\mathcal{G}(\theta_b, h(\theta_b)) = \left(\nabla_{\theta_{u_1}} F_{1,t,u}, \dots, \nabla_{\theta_{u_I}} F_{I,t,u} \right)^\top = 0. \quad (28)$$

According to Lemma 2, we discuss the Jacobian matrix of \mathcal{G} with respect to θ_u to show $h(\theta_b)$'s continuity, which is denoted by

$$\mathbf{J}_{\mathcal{G}} = \left[\nabla_{\theta_{u_i}, \theta_{u_j}}^2 F_{i,t,u}(\theta_b, \theta_u) \right]_{i,j=1}^I. \quad (29)$$

By Assumption 2 and the follower's second-order conditions (SOCs), we assert that $\mathbf{J}_{\mathcal{G}}$ is strictly diagonally dominant and thus non-singular, meeting the Lemma 2's conditions. With $h(\theta_b)$ established as continuous and Assumption 1, it follows that $F_{t,b}(\theta_b, h(\theta_b), I)$ is also continuous. For a discounted dynamic system, the continuity of the stage-game utility ensures that the corresponding discounted value function V_b is

also continuous with respect to θ_b [50]. Finally, since the value function V_b is continuous for each I , the leader's objective J_b – being a finite weighted sum of these continuous functions over the distribution $\mathbb{D}(I)$ – is itself continuous. With $J_b(\theta_b)$ confirmed as a continuous function over a compact set, the existence of an optimal universal leader policy θ_b^* is guaranteed [47]. Eventually, the combination of this optimal leader policy and the corresponding follower best responses constitutes an ESE.

APPENDIX B PROOF OF THEOREM 2

The mind map of the proof is illustrated in Fig. 11. It is worth noting that Eq. (16) in the main text describes a discrete time dynamical system, $\Theta^{(e+1)} = \Lambda(\Theta^{(e)})$. The FOCs of Definition 2 yield $\Omega(\Theta^*) = 0$, which implies $\Lambda(\Theta^*) = \Theta^*$, establishing the DSE profile Θ^* as a fixed point [51]. It is known from the theory of dynamical systems that if Λ represents a contraction mapping proximate to a fixed point (i.e., spectral radius $\rho(\nabla\Lambda) < 1$), then the system asymptotically converges to it [52]. We begin with some denotations and lemmas.

Lemma 3 (Theorem 1.20 of Ref. [53]). *Let $\mathbf{M} = \begin{bmatrix} \mathbf{A} & \mathbf{B} \\ \mathbf{B}^\top & \mathbf{D} \end{bmatrix}$ be a symmetric matrix, where \mathbf{A} is invertible. Then \mathbf{M} is negative definite, i.e., $\mathbf{M} \prec 0$, if and only if both $\mathbf{A} \prec 0$ and the Schur-complement $\mathbf{D} - \mathbf{B}^\top \mathbf{A}^{-1} \mathbf{B} \prec 0$.*

Lemma 4. *Let the symmetric part of the Jacobian of the scaled gradient vector field $\Omega(\Theta)$ evaluated at Θ as $\mathbf{M}(\Theta) = \frac{1}{2}(\mathbf{J}_\Omega(\Theta)^\top + \mathbf{J}_\Omega(\Theta))$. The Jacobian of this gradient field, $\mathbf{J}_\Omega(\Theta) = \nabla_{\Theta} \Omega(\Theta)$, evaluated at point Θ^* , is given by Eq. (30), where $\Omega_u = (\nabla_{\theta_{u_1}} J_{1,u}^{(e)}, \dots, \nabla_{\theta_{u_I}} J_{I,u}^{(e)})^\top$ is the followers part of gradient vector. We assure the block matrix $\mathbf{M}(\Theta^*)$ is negative definite.*

See Appendix C for the entire proof.

Next, we just need to show that $\rho(\nabla\Lambda) < 1$, i.e., considering its L_2 -norm. Taking the gradient of dynamic system $\nabla\Lambda(\Theta^*) = \mathbf{I} + \alpha_b \mathbf{J}_\Omega(\Theta^*)$, its squared L_2 -norm

$$\begin{aligned} & \|\mathbf{I} + \alpha_b \mathbf{J}_\Omega(\Theta^*)\|_2^2 \\ &= \sigma_{\max} \left((\mathbf{I} + \alpha_b \mathbf{J}_\Omega(\Theta^*))^\top (\mathbf{I} + \alpha_b \mathbf{J}_\Omega(\Theta^*)) \right) \\ &= \sigma_{\max} \left(\mathbf{I} + 2\alpha_b \mathbf{M}(\Theta^*) + \alpha_b^2 \mathbf{J}_\Omega^\top(\Theta^*) \mathbf{J}_\Omega(\Theta^*) \right) \\ &\stackrel{(a)}{\leq} 1 + 2\alpha_b \sigma_{\max}(\mathbf{M}(\Theta^*)) + \alpha_b^2 \sigma_{\max}(\mathbf{J}_\Omega^\top(\Theta^*) \mathbf{J}_\Omega(\Theta^*)) \\ &\stackrel{(b)}{=} \left(1 - \frac{\kappa_1^2}{\kappa_2} \right), \end{aligned}$$

where σ denotes the singular value. (a) implies Weyl's inequality [54]. Let $\kappa_1 = \sigma_{\min}(-\mathbf{M}(\Theta^*))$, $\kappa_2 = \sigma_{\max}(\mathbf{J}_\Omega^\top(\Theta^*) \mathbf{J}_\Omega(\Theta^*))$ and $\alpha_b = \frac{\kappa_1}{\kappa_2}$. By Lemma 4, $\mathbf{M}(\Theta^*) \prec 0$, its singular value are negative, so that both $\kappa_1, \kappa_2 > 0$. Furthermore,

$$\kappa_1^2 \leq \sigma_{\max}^2(-\mathbf{M}(\Theta^*)) \leq \sigma_{\max}(\mathbf{J}_\Omega(\Theta^*)^\top \mathbf{J}_\Omega(\Theta^*)) = \kappa_2, \quad (31)$$

$$\mathbf{J}_\Omega = \begin{bmatrix} \mathbf{J}_{11} & \mathbf{J}_{12} \\ \mathbf{J}_{21} & \mathbf{J}_{22} \end{bmatrix} = \left[\begin{array}{c|ccc} \nabla_{\theta_b}^2 J_b & \nabla_{\theta_{u_1}, \theta_b}^2 J_b & \cdots & \nabla_{\theta_{u_I}, \theta_b}^2 J_b \\ \hline \iota_u \nabla_{\theta_b, \theta_{u_1}}^2 J_{1,u} & \iota_u \nabla_{\theta_{u_1}}^2 J_{1,u} & \cdots & \iota_u \nabla_{\theta_{u_I}, \theta_{u_1}}^2 J_{1,u} \\ \vdots & \vdots & \ddots & \vdots \\ \iota_u \nabla_{\theta_b, \theta_{u_I}}^2 J_{I,u} & \iota_u \nabla_{\theta_{u_1}, \theta_{u_I}}^2 J_{I,u} & \cdots & \iota_u \nabla_{\theta_{u_I}}^2 J_{I,u} \end{array} \right] = \begin{bmatrix} \nabla_{\theta_b}^2 J_b^{(e)}(\Theta^*) & \nabla_{\theta_b, \theta_u}^2 J_b^{(e)}(\Theta^*) \\ \iota_u \nabla_{\theta_b} \Omega_u(\Theta^*) & \iota_u \nabla_{\theta_u} \Omega_u(\Theta^*) \end{bmatrix} \quad (30)$$

which means $\frac{\kappa_1^2}{\kappa_2} \in (0, 1)$, and we claim that (b) holds. Therefore, $\rho(\nabla \Lambda(\Theta^*)) \leq \sqrt{1 - \frac{\kappa_1^2}{\kappa_2}} < 1$, which establishes that $\nabla \Lambda(\Theta^*)$ is a contraction.

Consider the Taylor expansion of $\Lambda(\Theta)$ around Θ^* , we have

$$\begin{aligned} \|\Theta^{(e+1)} - \Theta^*\|_2 &= \|\Lambda(\Theta^{(e)}) - \Lambda(\Theta^*)\|_2 \\ &= \|(\mathbf{I} + \alpha_b \mathbf{J}_\Omega(\Theta^*))(\Theta_t - \Theta^*) + o(\Theta_t - \Theta^*)\|_2 \\ &\leq \|(\mathbf{I} + \alpha_b \mathbf{J}_\Omega(\Theta^*))\|_2 \|\Theta_t - \Theta^*\|_2 + \|o(\Theta_t - \Theta^*)\|_2 \\ &\approx \sqrt{1 - \frac{\kappa_1^2}{\kappa_2}} \|\Theta_t - \Theta^*\|_2. \end{aligned} \quad (32)$$

This leads to the geometric convergence rate $O(\sqrt{1 - \frac{\kappa_1^2}{\kappa_2}})$.

APPENDIX C PROOF OF LEMMA 4

Consistent with the formulation in Lemma 3, we first examine the sub-blocks of $\mathbf{M}(\Theta^*)$. The top-left block, $\mathbf{A} = \frac{1}{2}(\mathbf{J}_{11} + \mathbf{J}_{11}^\top) = \nabla_{\theta_b}^2 J_b^{(e)}(\Theta^*)$, is the Hessian of the BS with respect to its strategy parameters. Similarly, the bottom-right block $\mathbf{D}_\iota = \iota_u \mathbf{D} = \frac{1}{2}(\mathbf{J}_{22} + \mathbf{J}_{22}^\top)$, and its (j, k) -th sub-block is denoted by $\frac{\iota_u}{2}(\nabla_{\theta_{j,u}, \theta_{k,u}}^2 J_{j,u}^{(e)} + (\nabla_{\theta_{k,u}, \theta_{j,u}}^2 J_{k,u}^{(e)})^\top)$. From the SOCs of the underlying SDE, it is established that \mathbf{A} and the diagonal principal sub-blocks of \mathbf{D}_ι are negative definite. Assumption 2 stipulates that the norms of the cross second-order gradients between different UEs are negligible. Consequently, \mathbf{D}_ι is strictly diagonally dominant, which, in turn, implies that \mathbf{D}_ι is also negative definite. Off-diagonal block \mathbf{B} consists of the cross second-order gradient terms between the BS and the UEs, the norm of which is also assumed to be sufficiently small.

According to Lemma 3, it is now sufficient to demonstrate that $\mathbf{D}_\iota - \mathbf{B}^\top \mathbf{A}^{-1} \mathbf{B} \prec 0$. Let \mathbf{x} a non-zero vector, we analyze $\mathbf{x}^\top (\mathbf{D}_\iota - \mathbf{B}^\top \mathbf{A}^{-1} \mathbf{B}) \mathbf{x} < 0$ as follow:

$$\mathbf{x}^\top \mathbf{D}_\iota \mathbf{x} < \mathbf{x}^\top (\mathbf{B}^\top \mathbf{A}^{-1} \mathbf{B}) \mathbf{x} \quad (33a)$$

$$\Rightarrow \iota_u \sigma_{\min}(-\mathbf{D}) > \sigma_{\max}(-\mathbf{B}^\top \mathbf{A}^{-1} \mathbf{B}) \quad (33b)$$

$$\Rightarrow \iota_u \sigma_{\min}(-\mathbf{D}) > \|\mathbf{B}\|_2^2 \|\mathbf{A}^{-1}\|_2 \quad (33c)$$

$$\Rightarrow \iota_u \sigma_{\min}(-\mathbf{D}) \sigma_{\min}(-\mathbf{A}) > \|\mathbf{B}\|_2^2 \quad (33d)$$

Eq. (33b) leverages Rayleigh quotient properties [54] to establish singular value bounds for the matrix quadratic terms. Eq. (33c) then applies the submultiplicativity of the spectral norm [54], yielding $\sigma_{\max}(-\mathbf{B}^\top \mathbf{A}^{-1} \mathbf{B}) = \|\mathbf{B}^\top \mathbf{A}^{-1} \mathbf{B}\|_2 \leq \|\mathbf{B}\|_2^2 \|\mathbf{A}^{-1}\|_2$. Eq. (33d) involves substituting the identity $\|\mathbf{A}^{-1}\|_2 = \sigma_{\min}^{-1}(-\mathbf{A})$ into Eq. (33c). An appropriate choice of ι_u then ensures the resulting inequality holds. Therefore, the Schur complement of $\mathbf{M}(\Theta^*)$ is also negative definite, confirming that $\mathbf{M}(\Theta^*)$ itself is negative definite.

APPENDIX D PROOF OF COROLLARY 1

In the dynamic MFSG with stochastically varying followers, the epoch-wise gradient field is formulated as

$$\Omega(\Theta^{(e)}, \bar{I}_e) = \left(\nabla_{\theta_b} J_b^{(e)}, \iota_u \left(\frac{1}{\bar{I}_e} \sum_{i=1}^{\bar{I}_e} \nabla_{\theta_u} J_{i,u}^{(e)} \right) \right)^\top, \quad (34)$$

where \bar{I}_e denotes the batch-wise expected number of followers. For convergence analysis, Eq. (16) is rewritten as the average dynamics

$$\Theta^{(e+1)} = \Theta^{(e)} + \alpha_b \cdot \bar{\Omega}(\Theta^{(e)}), \quad (35)$$

where $\bar{\Omega}(\Theta) = \mathbb{E}_{\bar{I}_e \sim \mathbb{D}(I)}[\Omega(\Theta, \bar{I}_e)]$ is the averaged gradient vector. The pivotal step in the proof of Theorem 2 is showing that the symmetric part of the Jacobian $\bar{\mathbf{M}}(\Theta^*)$ is negative definite. Here, this key variable also transforms into its expected form.

$$\bar{\mathbf{M}}(\Theta^*) \triangleq \mathbb{E}_{\bar{I}_e} [\mathbf{M}(\Theta^*, \bar{I}_e)]. \quad (36)$$

Lemma 4 ensures that $\mathbf{M}(\Theta^*, I)$ is negative definite for any realization I . Since expectations over the distribution are convex combinations of these matrices and the cone of negative definite matrices is convex, it follows that $\bar{\mathbf{M}}(\Theta^*)$ is negative definite. Let $\kappa_1 = \sigma_{\min}(-\bar{\mathbf{M}}(\Theta^*))$ and $\kappa_2 = \sigma_{\max}(\bar{\mathbf{J}}_\Omega(\Theta^*)^\top \bar{\mathbf{J}}_\Omega(\Theta^*))$, we obtain a convergence result similar to Theorem 2. Crucially, the validity of this entire analysis hinges on the LLM-enabled universal policy, whose fixed-dimensional parameter space Θ renders the expectation over Jacobians from different game instances mathematically coherent.